Electrochemical Engineering Considerations for Gas Evolution in Molten Sulfide Electrolytes

by

Brian John Chmielowiec

S.B., Massachusetts Institute of Technology (2012)
M.S., California Institute of Technology (2014)

Submitted to the Department of Materials Science and Engineering
in partial fulfillment of the requirements for the degree of

Doctor of Science

at the

MASSACHUSETTS INSTITUTE OF TECHNOLOGY

June 2019

Author .... Signature redacted
.....
Department of Materials Science and Engineering
May 16, 2019

Certified by... Signature redacted
.....
Antoine Allanore
Associate Professor of Metallurgy
Thesis Supervisor

Accepted by ..... Signature redacted
Donald R. Sadoway
John F. Elliott Professor of Materials Chemistry
Chairman, Department Committee on Graduate Theses

Electrochemical Engineering Considerations for Gas Evolution in Molten Sulfide Electrolytes

by

Brian John Chmielowiec

Submitted to the Department of Materials Science and Engineering
on May 16, 2019, in partial fulfillment of the
requirements for the degree of
Doctor of Science

Abstract

The current interrupt and galvanostatic electrochemical impedance spectroscopy techniques were utilized to characterize the ohmic, charge transfer, and mass transfer overpotential behavior of gas evolving electrodes in aqueous, molten chloride, and molten sulfide electrolyte solutions under steady-state natural convective flow conditions as a means to gain access to thermodynamic, physicochemical, and hydrodynamic properties of these systems. Previous efforts purposely chose operating conditions under which one or more sources of overpotential were negligible to facilitate analysis of the total overpotential observed at the expense of maintaining operating conditions of industrial relevance.

This work represents a preliminary effort to understand the fundamental material properties of a molten sulfide electrolyte, by application of materials-blind electrochemical techniques that were validated on previously well characterized systems-oxygen evolution in aqueous KOH and chlorine evolution in eutectic LiCl-KCl-CsCl.

For the first time, values are reported for the saturation concentration of dissolved sulfur gas, an approximate range of Schmidt number for dissolved sulfur, and natural convection limiting current densities in a molten sulfide electrolyte consisting of Cu_2S-BaS-La_2S_3 at 1300°C.

Thesis Supervisor: Antoine Allanore
Title: Associate Professor of Metallurgy

Acknowledgments

First I must thank my parents, Dennis and Sue, for all of the love and support that you have given me. I would have never made it this far without you. Also, my sister, Katie, for always setting a standard of excellence for which I could only strive to achieve.

My wife, Lucy: you've been by my side everyday of this long arduous journey that is a PhD. There were many ups and downs during this journey, but one thing remained constant- your support.

Professor Allanore, for twice taking a chance on me, once as a UROP back in 2010, and again as a graduate student in 2014. Your unwavering technical and professional support kept this thesis on track and your appetite for pushing the frontier of our scientific knowledge was truly motivational.

Professor Fukunaka, for convincing me to travel all the way to Japan to record videos of bubbles evolving from various surfaces. I am truly grateful for the international experiences and relationships that I developed as a result of the JSPS fellowship.

Hilary, for all the unacknowledged work behind the scenes that you do to keep the Allanore Group running like a well oiled machine.

John, for always stopping by to take care of us in the building 13 labs, no matter how "busy, busy" you were. A clean work space is something that shouldn't be taken for granted.

Lastly, all the researchers in the Allanore Group, with whom I had the honor of working in the trenches every day. What makes MIT such a special place is the people, and this group was no exception.

Contents

List of Figures

List of Tables

Chapter 1

Introduction

The United Nations predicts that the global population will increase by 2 billion people by the year 2050 relative to today.[1] Such population growth challenges existing production methods for food, clean water, energy, and materials. The Intergovernmental Panel on Climate Change expects the global energy consumption to double relative to 2001 conditions. Ijima and coworkers have extensively studied and forecasted the consumption of metals to 2050 and in many cases found that demand will grow by much more than twice the current levels.[2] World usage of common base metals (Fe, Al, Cu, Ni, Pb, and Zn) was ~1.6 billion metric tons in 2016.[3–8] With the exception of gold and platinum group metals (and to a much smaller extent, silver and copper) which are more commonly found in their native state, all metals are primarily extracted from their mined ores.[9] Despite incremental improvements in efficiency, the pyrometallurgical processing for many metals such as Cu is the same as the one developed in antiquity.[10] Consequentially, this means there are unsatisfactorily large amounts of waste (low value slags, waste water, CO_2, etc) associated with production of these metals. Figure 1-1 shows the cradle to gate emissions associated with the current extraction processes for steel, Al, Cu, Pb, Zn, and Ni. The starting materials (ore vs concentrate) and final state of the metal product can be found in reference [11]. Thus to meet the aforementioned unprecedented demand for metals and the desire for their sustainable production, a fundamental shift in processing of metal ores is required. This shift is possible via an *innovation in materials* used to

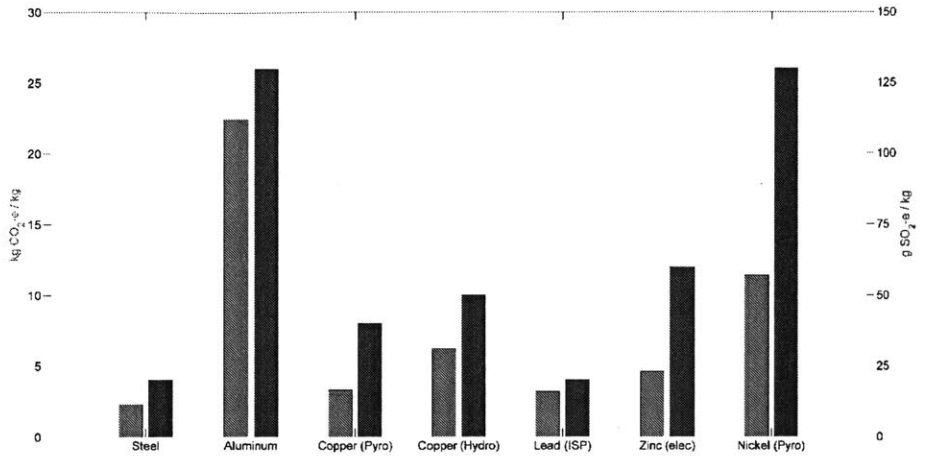

Figure 1-1: Cradle-to-gate emissions of some commodity metals. Pyro=pyrometallurgical, Hydro=hydrometallurgical, ISP=Imperial smelting process, and elec=electrolysis

extract metals from their ores.

The Hall-Héroult process is a classic example of how a materials innovation allowed for aluminum, a metal as precious as silver in the late 1800s, to become a commodity metal. The materials innovation of course was the use of cryolite, an amazing supporting electrolyte that enabled production of liquid aluminum at the cathode and CO_2 gas at the carbon anode. Modern aluminum smelters have capacities as large as 500kta, running at cathodic current densities of $8kA/m^2$. With the recent development of an inert anode technology by Alcoa and Rio Tinto [12], the ability to use electrons as the sole reductant for the electrowinning of Al will greatly curtail associated CO_2 emissions. As renewables (solar, wind, etc) continue to displace fossil fuels in the energy production sector, the ability to use carbon-free electricity to decompose metallic ores offers a unique opportunity for pollution-free metal production via electrolysis.[13]

Due to the commodity nature of many metals, the driving factor in choice of production method has been cost. Consequentially, all of the metals mentioned above are produced in the molten state which allows for the highest levels of productivity. Thus to compete with the cost of current pyrometallurgical methods of extraction [14, 15],

it is foreseen that any new extraction process must also be able to produce liquid metal in a continuous or semi-continuous fashion. However, to also satisfy the need for sustainability and limit/prevent any release of greenhouse and acid gases (e.g. CO_2, SO_x, ...), effective separation of the nonmetal component of the ore in its elemental form must be designed. The greatest opportunity for innovation corresponds to the sulfide-class of ores, which represent ~60% of all minerals. Cu, Mo, Re, Pb, Zn, Ag, Cd, and Ni are all found predominantly as sulfide bearing ores and represent significant economic value. Agnostic to the metal cation present in the ore, the pyrometallurgical approach of roasting the metal sulfide to produce either metal oxide or native metal results in generation of SO_2 which must be captured and converted to sulfuric acid. For example, during the roasting of chalcopyrite ($CuFeS_2$), approximately three tons of SO_2 per ton of copper metal are produced. The process of capturing and converting the SO_2 into sulfuric acid requires significant capital investment: 25% and 12.5% of the smelter's fixed and operating costs, respectively.[10]

In essence, a new medium is needed in which to facilitate the decomposition of the metal sulfide, MS_z into its elemental components, M and S_2:

$$MS_{x(\ell,s)} \rightarrow M_{(\ell)} + \frac{x}{2} S_{2(g)} \tag{1.1}$$

while bypassing the wastes associated with pyrometallurgy.

1.1 The electrolytic approach

The Hall-Héroult process, as mentioned above, illustrates a commercial implementation of electrolysis to perform the extraction of metal from its ore. Molten oxide electrolysis (MOE), first championed by Sadoway in the early 1990s[16–19], utilizes the same operating principles as Al electrowinning to produce liquid iron or iron alloys at the cathode and carbon monoxide gas at the (carbon) anode. The development of a non-noble metal inert anode allows for the potentially economic evolution of oxygen instead of carbon monoxide.[20] Like the Hall-Héroult cell, MOE affords many of the

advantages of operating in the molten state, namely:

- high solubility of feedstock into the supporting electrolyte
- low kinetic barrier to Faradaic reactions
- high rates of mass transport of reactants and products (limiting current densities $> 2\text{A/cm}^2$)
- liquid metal production

Again, the supporting electrolyte, commonly a mixture of silica and reactive[1] metal oxides, was the enabling material innovation. Could a similar innovation in electrolyte material enable a renaissance in how metal sulfides are decomposed to meet growing demand and sustainability goals?

While MOE has the benefit of building off the knowledge acquired in geology and the glass industry, MSE can also benefit from the geology community, which often deals with sulfide-based liquid magma. The flow of information is by no means one way. In a 2010 report, the Earth Resources Engineering Section of the National Academy of Engineering outlined "specific challenges" to achieve the "grand challenge" of "[supplying] society with its essential needs for energy, minerals and groundwater, and to use the earth itself as a resource for protecting people and the environment." Two of these specific challenges are to "understand, engineer and control subsurface coupled processes" and to "make the earth transparent." The report identifies the need to understand subterranean fluid flow as well as the thermal, mechanical, chemical, and biological processes occurring below the earth's surface. Given the vast amount of volcanogenic massive sulfide deposits, any information regarding the hydrodynamic behavior of sulfide mattes can benefit the geology community. Elemental partitioning between slag and matte phases is dependent on the thermodynamic stability of each element in the oxygen and sulfur rich phases. Fluid flow is typically governed by a set of dimensionless properties such as the Reynolds number (in forced convection), the Rayleigh number (in free convection), and the Schmidt

[1]here, reactive indicates a metal which can reduce silicon from its oxide

number (ratio of mass diffusivity to kinematic viscosity). When dealing with heterogeneous processes such as the exchange of heat and mass between two immiscible liquids or charge transfer at an electrode surface, the surface tensions of the various materials involved can greatly influence the observed behavior. There still exists a need to quantify the thermodynamic, hydrodynamic, and physicochemical properties of many existing high temperature molten materials as well as exploratory materials under development. Molten sulfide electrolysis (MSE) offers a paradigm shift in the way metals can be won from their native ores by utilizing a supporting electrolyte composed of other molten sulfides. Equations 1.1-3 describes the ideal conversion of metal sulfide (MS_x) to metal (M) and elemental sulfur (S_2) at the cathode and anode, respectively.

$$M^{2x+}_{(dis)} + 2xe^- \rightarrow M_{(l,s)} \tag{1.2}$$

$$xS^{2-}_{(dis)} \rightarrow \frac{x}{2}S_{2(g)} + 2xe^- \tag{1.3}$$

$$MS_{x(l,s)} \rightarrow M_{(l,s)} + \frac{x}{2}S_{2(g)} \tag{1.4}$$

If this conversion is carried out with electrons, there are no additional byproducts (wastes). This method benefits from many of the same advantages of Molten Oxide Electrolysis (MOE), namely a high productivity rate (>10kA/m^2), production of liquid metal, environmentally benign (and condensible) anodic product, and semi-continuous operation (periodic tapping of metallic product prevents fully continuous operation). With the surge of clean renewable production of electricity, an extractive approached utilizing only electrical work can perhaps meet *sustainability* goals.

1.1.1 Previous efforts to electrolyze transition metal sulfides

Transition metal sulfides are liquid semiconductors. They exhibit electrical conductivities on the range 10^2-$5{\cdot}10^5$S/m. For comparison, molten salts, have electrical conductivities < 1S/m with ionic transference numbers much, much closer to unity. Due to their high electronic transference numbers, transition metal sulfides have thwarted direct electrochemical decomposition on an industrial scale.

The electrochemical decomposition of metal sulfides in the molten state was first demonstrated in 1906 by Townsend [21], and separately by Valentine and Betts.[22] These initial studies focused on the electrowinning of lead from molten galena in contact with a molten salt mixture of plumbous chloride and sodium chloride. This design was reinvigorated by Sadoway for the purpose of electrowinning antimony from stibnite (Sb_2S_3).[23] The operating principle behind these early electrolysis setups is that due to mutual immiscibility and density differences, the system will naturally separate due to the force of gravity into three distinct layers: the metal halide phase (lowest density) rests above the metal sulfide phase (intermediate density) which rests above the electrowon metal (highest density). This configuration neutralizes the issue of electronic conductivity inherent to the sulfide phase because the molten chloride layer acts as an electron blocker, allowing only ionic current to pass. The limitations of this methodology are twofold. First, the solubility of sulfides in halides is limited, which results in a limited anodic current density for sulfur evolution.[24] Chlorine evolution begins to compete with sulfur evolution as the current density increases. The competition between oxidation of sulfide and chloride anions is impermissible as the supporting electrolyte should not need to be replenished at the same rate as the feedstock ore. Second, chemical reaction between the chloride and sulfide phases is possible, especially at higher temperatures.

An alternative high temperature approach that found traction in the literature was the use of solid metal sulfide anodes in molten chlorides.[25–27] The motivation behind this approach was that many sulfides with high melting points tend to decompose before melting. The sulfide ions in the compound were oxidized to sulfur gas and the metal cations were liberated to the chloride melt. This configuration also suffered from poor mass transport, chlorine co-evolution, and the formation of a non-conductive layer on the anode.

A distinctly different melt chemistry (free of halides) is found in the Na-S high temperature battery. Newman [28, 29] performed extensive work modelling the transport within this system of sodium polysulfides, particularly regarding the transference number and diffusivities of these melts. Newman was able to find Arrhenius-type de-

pendence of the diffusivity, which is also commonly found in chloride and fluoride melts [30, 31] and also argued for the applicability of the Nernst-Einstein relation and Stokes-Einstein relation for the sodium sulfide melts. The applicability of the Stokes-Einstein equation to describe the melt viscosity is somewhat surprising, but suggests the lack of network formers which cause glass-like melts to deviate from Stokes-Einstein behavior.[32]

1.1.2 Copper molten sulfide electrolysis shows promise

To circumvent the previous issues encountered in the electrolysis of metal sulfides, the Allanore group has designed an all sulfides molten electrolyte. Sokhanvaran demonstrated the feasibility of conducting faradaic reactions in a molten mixture of cuprous sulfide (Cu_2S) and barium sulfide (BaS).[33] Molten Cu_2S, with an electrical conductivity of 4700S/m at the melting temperature cannot be decomposed electrolytically in the pure state. BaS, with a band gap of 3.92eV [34] suppresses the electronic conductivity of the melt when mixed with cuprous sulfide as evidenced by the completion of faradaic reactions. Cann [35] measured the change in ionic and electronic transference numbers as both functions of temperature and composition and indeed showed that increasing the BaS content allowed for faradaic reactions to occur. An immiscibility gap centered around 20mol% Cu_2S suggests that electronic conductivity can be severely mitigated when the Cu_2S concentration is <20mol%.[36] Sahu [37] even showed selective reduction of Cu, Mo, and Re (which commonly exist in ores) in a molten sulfide electrolyte. Efficiencies as high as 70% have been measured which further justify the research effort to properly characterize molten sulfide as potential materials for pollution-free extraction of metal.

1.2 Considerations from electrochemical engineering

Norbert Ibl, one of the founding fathers of electrochemical engineering, noted [38] "the goal of electrochemical engineering is to achieve, in a quantitative way, an optimal cell design." Without knowledge of the thermodynamic and hydrodynamic behavior of

the system components, the informed design of reactors is virtually hopeless. Given the potential of high temperature liquid state electrochemical processing to meet impending sustainability requirements, the author would like to focus on the desired properties of a suitable electrolyte. Of course, some of these properties are relevant outside of the context of electrochemical design. A suitable supporting electrolyte, for the purpose of electrowinning a metal from its ore or concentrate shall have the following properties:

- high ionic conductivity, typically >1S/cm with correspondingly low electronic conductivity
- low vapor pressure, typically less than 100Pa at the operating temperature
- wide electrochemical window, wide enough to ensure negligible decomposition of the supporting electrolyte
- high solubility of feed stock, typically greater than a few weight percent
- high productivity, typical current densities >1A/cm^2
- low solubility of products, both metal and gas in the supporting electrolyte

Fortunately, the search for this ideal novel electrolyte material does not need to start from scratch. While until now, an electrolyte system with *all* of the above properties has remained elusive, materials with some of the desired properties have been found and can guide the discovery of the ideal candidate.

1.2.1 Considerations from the smelting industry

Given the maturity of the copper smelting industry, much about physical properties can be learned from the pyrometallurgists. Several texts review the operating principles behind the pyrometallurgical approach to winning metals from their ores [14, 15] with Davenport's text [10] focusing specifically on the extractive metallurgy of copper. Electrical conductivity data of mattes were measured by Pound [39] and Liu [40]. Nikiforov measured matte viscosities.[41] Shimpo provided key insights into structure

and the equilibrium between matte and slag.[42] Data regarding the interaction of gas with matte in the Pierce-Smith converter however remain lacking.

1.3 More considerations from the field of electrochemical engineering

One would be remiss to overlook the contributions of Wagner, Tobias, Hine, and Ibl to the field of electrochemical engineering.[43–52] These researchers are considered the fathers of electrochemical engineering. Ibl eloquently points out in a paper from 1959 [50] that when considering mass transfer in electrochemical cells, three dimensionless numbers always arise from the analysis: the Sherwood number (Sh), the Schmidt number (Sc), and the Grashof number (Gr). Carl Wagner is responsible for yet another dimensionless number which bears his name- the Wagner number (Wa).

The value of the Sherwood number ultimately determines the rate of convective mass transport to and away from the electrode surface. The product of the Grashof and Schmidt numbers is called the mass Rayleigh number (Ra_m) and is frequently found in correlations describing natural convection. In addition to the authors above, Fukunaka [53–55], and Vogt [56–59] have investigated natural convection and more specifically electrolytic bubble evolution quite extensively, validating correlations of the mass transfer coefficient via spectroscopic and idiometric means in aqueous solutions.

The power of describing electrochemical phenomena with these dimensionless numbers is that by carefully designing an electrochemical reactor that is sufficiently similar (geometrically, thermally, and electrically) to the experimental apparatus used to establish the correlations, one can gain insight that would otherwise not be possible via direct measurement. This is of tremendous utility in the case of MSE, because many hydrodynamic and thermodynamic properties of these materials are unknown, but by performing electrochemical measurements, the properly non-dimensionalized response can be compared with data collected from other systems with well-known

physical parameters, i.e. aqueous systems and molten salt systems.

The last major electrochemical engineering aspect to be covered is of course the energy balance, and how energy input depends on the dimensionless parameters previously defined, and ultimately, the current density. Embracing the approach by Stender for sodium chloride electrolysis [60], Equation 1.5 highlights the main contributions to the total cell voltage, E_{cell}, where E_{min} is the minimum thermodynamic decomposition potential, η_{iR} is the ohmic overpotential due to current flow through the electrochemical cell, η_{ct} is the charge transfer overpotential which is related to the kinetics of the decomposition reaction, and η_{mt} is due to mass transport limitations.

$$E_{cell} = E_{min} + \eta_{iR} + \eta_{ct} + \eta_{mt} \tag{1.5}$$

For systems which evolve gas at one or both electrodes, η_{mt} has been shown to be dominated by the transport of gas to/from the electrode surface.[61–63] Preliminary results in copper MSE also suggest this to be the case.

The current interrupt technique has been classically used to measure ohmic overpotential. [54, 64, 65] With the vast improvements in computational power, alternating current methods have come to largely replace the current interrupt technique.[66, 67] Electrochemical Impedance Spectroscopy (EIS), with its ability to perturb the electrochemical system in a range of frequencies can be used to measure both ohmic overpotential and charge transfer overpotential, which is particularly necessary in low temperature systems which are usually kinetically limited. Lastly, alternating current voltammetry (ACV), has demonstrated tremendous utility in measuring not only kinetic, but also thermodynamic properties of electrochemical reactions. The interest reader should look at references [68, 69] for thorough reviews of these above techniques. One of the great features of electrochemical methods, is that they can be applied at virtually any temperature and environment, provided material compatibility be maintained. This feature is key in order to connect the overpotential between systems as diverse as aqueous electrolytes, molten salts, molten oxides, and molten sulfides and correlate the electrochemical signals to hydrodynamic (mass transfer

coefficients), physicochemical (Sc), and thermodynamic properties (gas saturation concentrations) of the different systems.

1.4 Focus of the present work

Heterogeneous gas evolution is a prevalent feature of many present-day electrolytic processes as well as for future technologies such as MOE and MSE. The chemistry of oxygen in aqueous electrolytes is very well understood. To a lesser extent, the chemistry of chlorine in molten salts and oxygen in molten oxides has been studied. Knowledge of the chemical interaction of sulfur in molten sulfide melts is almost non-existent. Recently, Caldwell [70] showed the value in coupling electrochemical techniques in situ with models of mass transfer to understand the role of oxygen and the supporting electrolyte that enabled current densities $>2A/cm^2$ to be observed during MOE. Therefore the present work seeks to characterize novel sulfide-based electrolytes using, when applicable, the techniques already developed for aqueous and molten electrolyte systems to characterize the chemical and/or hydrodynamic behavior that fundamentally limits the electrochemistry of sulfur evolution in molten sulfides. Such techniques, which will be discussed in the next chapter, include current interrupt, galvanostatic electrochemical impedance spectroscopy, and alternating current voltammetry.

1.5 Summary

The need for a paradigm shift in processing technology was identified for the sustainable production of metals, particularly those that form predominantly sulfide ores. High temperature based processes operating in the molten state were shown to have key advantages, enabling high productivity. Processing sulfide based ores in the molten phase to electrowin the metal was suggested as an ideal path towards sustainability. Molten sulfides, as a class of materials, are woefully understudied and the need for measurement of thermodynamic, hydrodynamic, and, physicochemical

properties of these molten materials was identified as critical for the understanding of the fundamental electrochemical processes at work during MSE. Electrochemical techniques utilized for the measurement of relatively low temperature materials were identified. Extension of these techniques to measure high temperature molten data under extreme conditions was suggested. By correlating the electrochemical behavior of well-characterized, low temperature systems to their physical properties, and application of these same techniques to novel sulfide-based electrolytes, it is foreseen to help characterize MSE systems in situ under their challenging operating conditions.

References

[1] "World Population Prospects: The 2017 Revision, Key Findings and Advance Tables," tech. rep., United Nations, New York, 2017.

[2] K. Halada, M. Shimada, and K. Ijima, "Forecasting the Consumption of Metals up to 2050," *Materials Transactions*, vol. 49, no. 3, pp. 402–410, 2008.

[3] World Steel Association, "Iron ore production worldwide in 2016 by region (in million metric tons)," tech. rep., 2016.

[4] KPMG, "Global aluminum consumption from 2013 to 2016 (in million metric tons)," tech. rep., 2016.

[5] International Copper Study Group, "Refined copper usage worldwide from 2007 to 2017 (in 1,000 metric tons)," tech. rep., 2017.

[6] Norilsk Nickel, "Global consumption of nickel from 2009 to 2017 (in 1,000 metric tons)," tech. rep., 2017.

[7] International Lead and Zinc Study Group, "World lead consumption from 2004 to 2017 (in 1,000 metric tons)," tech. rep., 2017.

[8] International Lead and Zinc Study Group, "Global consumption of zinc from 2004 to 2017 (in 1,000 metric tons)," tech. rep., 2017.

[9] R. L. Lowrie, *SME mining reference handbook*. 2002.

[10] W. Davenport, M. King, M. Schlesinger, and A. Biswas, *Extractive Metallurgy of Copper*. Elsevier Ltd, 4th ed., 2002.

[11] T. E. Norgate, S. Jahanshahi, and W. J. Rankin, "Assessing the environmental impact of metal production processes," *Journal of Cleaner Production*, vol. 15, no. 8-9, pp. 838–848, 2006.

[12] Elysis, "Rio Tinto and Alcoa announce world's first carbon-free aluminium smelting process," 2018.

[13] A. Allanore, "Features and challenges of molten oxide electrolytes for metal extraction," *Journal of the Electrochemical Society*, vol. 162, no. 1, pp. E13–E22, 2015.

[14] C. B. Gill, *Non-ferrous Extractive Metallurgy.* New York: John Wiley & Sons Inc., 1980.

[15] T. Rosenqvist, *Principles of Extractive Metallurgy.* Trondheim: Tapir Academic Press, 2nd ed., 2004.

[16] D. R. Sadoway, "The electrochemical processing of refractory metals," *JOM*, vol. 43, no. 7, pp. 15–19, 1991.

[17] D. R. Sadoway, "Apparatus and method for the electrolytic production of metals," 1991.

[18] D. R. Sadoway, "Electrolytic production of metals using consumable anodes," 1993.

[19] D. R. Sadoway, "Apparatus for the electrolytic production of metals," 1993.

[20] A. Allanore, L. Yin, and D. R. Sadoway, "A new anode material for oxygen evolution in molten oxide electrolysis," *Nature*, vol. 497, no. 7449, pp. 353–356, 2013.

[21] C. P. Townsend, "Process for the Reduction of Ores," 1906.

[22] W. Valentine and A. G. Betts, "Process of Smelting Lead Ores," 1906.

[23] H. Yin, B. Chung, and D. R. Sadoway, "Electrolysis of a molten semiconductor," *Nature Communications*, vol. 7, pp. 1–5, 2016.

[24] O. P. Mohapatra, C. B. Alcock, and K. T. Jacob, "Solubilities of Pb2+,Bi3+, Sb3+, and Cu1+ sulfides in (NaCl- KCl-Na2S) melts," *Metallurgical Transactions*, vol. 4, pp. 1756–1762, 1973.

[25] T. Wang, H. Gao, X. Jin, H. Chen, J. Peng, and G. Z. Chen, "Electrolysis of solid metal sulfide to metal and sulfur in molten NaCl-KCl," *Electrochemistry Communications*, vol. 13, no. 12, pp. 1492–1495, 2011.

[26] S. Venkatachalam, "Treatment of chalcopyrite concentrates by hydrometallurgical techniques," *Minerals Engineering*, vol. 4, no. 7-11, pp. 1115–1126, 1991.

[27] X. Ge, X. Wang, and S. Seetharaman, "Copper extraction from copper ore by electro-reduction in molten CaCl2-NaCl," *Electrochimica Acta*, vol. 54, no. 18, pp. 4397–4402, 2009.

[28] T. Risch and J. Newman, "Transference Number Calculations for Sodium Polysulfides," *Journal of The Electrochemical Society*, vol. 135, no. 7, pp. 1715–1720, 1988.

[29] S. D. Thompson and J. Newman, "Differential Diffusion Coefficients of Sodium Polysulfide Melts," *Journal of The Electrochemical Society*, vol. 136, no. 11, pp. 3362–3371, 1989.

[30] A. M. Popescu and V. Constantin, "Viscosity of Alkali Fluoride Ionic Melts at Temperatures up to 373.15 K above Melting Points," *Chemical Engineering Communications*, vol. 202, no. 12, pp. 1703–1710, 2014.

[31] A. Z. Borucka, B. J. O'M, and J. A. Kitchener, "Self-diffusion in molten sodium chloride: a test of the applicability of the Nernst - Einstein equation," *Proceedings of the Royal Society of London. Series A, Mathematical and Physical Sciences*, vol. 241, no. 1227, pp. 554–567, 1957.

[32] J. A. Hodgdon and F. H. Stillinger, "Stokes-Einstein violation in glass-forming liquids," vol. 48, no. 1, pp. 1–7, 1993.

[33] S. Sokhanvaran, S.-K. Lee, G. Lambotte, and A. Allanore, "Electrochemistry of Molten Sulfides: Copper Extraction from BaS-Cu2S," *Journal of The Electrochemical Society*, vol. 163, no. 3, pp. D115–D120, 2016.

[34] T. Lv, D. Chen, and M. Huang, "Quasiparticle band structures of BaO and BaS," *Journal of Applied Physics*, vol. 100, no. 8, pp. 0861031–0861033, 2006.

[35] J. Cann, *Methodology for Determining Electronic Transference Numbers in Molten Sulfide Melts.* PhD thesis, 2017.

[36] C. Stinn, K. Nose, T. Okabe, and A. Allanore, "Experimentally Determined Phase Diagram for the Barium Sulfide-Copper(I) Sulfide System Above 873 K (600C)," *Metallurgical and Materials Transactions B*, vol. 48, no. 6, pp. 2922–2929, 2017.

[37] S. K. Sahu, B. Chmielowiec, and A. Allanore, "Electrolytic Extraction of Copper , Molybdenum and Rhenium from Molten Sulfide Electrolyte," *Electrochimica Acta*, no. 243, pp. 382–389, 2017.

[38] V. Stankovic, "Electrochemical Engineering - its appearance, evolution and present status. Approaching an anniversary.," *Journal of Electrochemical Science and Engineering*, vol. 2, no. 2, pp. 53–66, 2012.

[39] G. M. Pound, G. Derge, and G. Osuch, "Electrical conduction in molten copper-iron sulfide mattes," *Journal of Metals*, vol. 7, pp. 481–484, 1955.

[40] C. Liu, M. Chang, and A. He, "Specific conductance of Cu2S Ni2S3, and commercial matte," *Chinese Nonferrous Metals*, vol. 32, no. 1, pp. 76–78, 1980.

[41] L. V. Nikiforov, V. A. Nagiev, and V. P. Grabchak, "Viscosity of sulfide melts," *Inorganic Materials*, vol. 12, pp. 985–988, 1976.

[42] R. Shimpo, S. Goto, O. Ogawa, and I. Asakura, "A study on the equilibrium between copper matte and slag," *Canadian Metallurgical Quarterly*, vol. 25, pp. 113–121, 1986.

[43] C. Wagner, "Theoretical Analysis of the Current Density Distribution in Electrolytic Cells," *Journal of The Electrochemical Society*, vol. 98, no. 3, p. 116, 1951.

[44] C. Wagner, "Current Distribution in Galvanic Cells Involving Natural Convection," *Journal of The Electrochemical Society*, vol. 104, no. 2, p. 129, 1957.

[45] C. Wagner, "Contribution to the Theory of Current Distribution in Local Cells," *Journal of The Electrochemical Society*, vol. 107, no. 5, p. 445, 1960.

[46] C. Wagner, "Potential and current distribution at electrodes with local variations of the polarization parameter," *Electrochimica Acta*, vol. 12, no. 2, pp. 131–136, 1967.

[47] R. E. Meredith and C. W. Tobias, "Conduction in heterogeneous systems," *Advances in Electrochemistry and Electrochemical Engineering*, vol. 2, pp. 15–47, 1962.

[48] R. E. Davis, G. L. Horvath, and C. W. Tobias, "The Solubility and Diffusion Coefficient of Oxygen in Potassium Hydroxide Solutions," *Electrochimica Acta*, vol. 12, pp. 287–297, 1967.

[49] F. Hine, *Electrode Processes and Electrochemical Engineering.* New York and London: Plenum Press, 1985.

[50] N. Ibl, "The Use of Dimensionless Groups in Electrochemistry," *Electrochim. Acta*, vol. 1, pp. 117–129, 1959.

[51] N. Ibl, "Optimization of copper refining," *Electrochimica Acta*, vol. 22, no. 4, pp. 465–477, 1977.

[52] N. Ibl, "Fundamentals of Transport Phenomena in Electrolytic Systems," in *Comprehensive Treatise of Electrochemistry*, pp. 1–63, 1983.

[53] S. Kawai, Y. Fukunaka, and S. Kida, "Numerical Simulation of Transient Natural Convection along Vertical Plane Electrodes Caused by Electrolytic Current Modulation," *Journal of The Electrochemical Society*, vol. 155, no. 5, pp. F75–F81, 2008.

[54] H. Matsushima, D. Kiuchi, Y. Fukunaka, and K. Kuribayashi, "Single bubble growth during water electrolysis under microgravity," *Electrochemistry Communications*, vol. 11, no. 8, pp. 1721–1723, 2009.

[55] Y. Fukunaka, K. Suzuki, A. Ueda, and Y. Kondo, "Mass-Transfer Rate on a Plane Vertical Cathode with Hydrogen Gas Evolution," *Journal of The Electrochemical Society*, vol. 136, no. 4, pp. 1002–1009, 1989.

[56] H. Vogt, "The rate of gas evolution of electrodes-I. An estimate of the efficiency of gas evolution from the supersaturation of electrolyte adjacent to a gas-evolving electrode," *Electrochimica Acta*, vol. 29, no. 2, pp. 167–173, 1984.

[57] H. Vogt, "On the gas-evolution efficiency of electrodes. I - Theoretical," *Electrochimica Acta*, vol. 56, no. 3, pp. 1409–1416, 2011.

[58] H. Vogt, "On the gas-evolution efficiency of electrodes. II - Numerical analysis," *Electrochimica Acta*, vol. 56, no. 5, pp. 2404–2410, 2011.

[59] R. J. Balzer and H. Vogt, "Effect of Electrolyte Flow on the Bubble Coverage of Vertical Gas-Evolving Electrodes," *Journal of The Electrochemical Society*, vol. 150, no. 1, p. E11, 2003.

[60] W. W. Stender, P. B. Zivotinsky, and M. M. Stroganoff, "The Voltage Balance of a Cell for the Electrolysis of Sodium Chloride Solutions," *Transactions of The Electrochemical Society*, vol. 65, no. 1, pp. 189–213, 1934.

[61] H. Matsushima, T. Iida, and Y. Fukunaka, "Gas bubble evolution on transparent electrode during water electrolysis in a magnetic field," *Electrochimica Acta*, vol. 100, pp. 261–264, 2013.

[62] H. Matsushima, D. Kiuchi, and Y. Fukunaka, "Measurement of dissolved hydrogen supersaturation during water electrolysis in a magnetic field," *Electrochimica Acta*, vol. 54, no. 24, pp. 5858–5862, 2009.

[63] S. Shibata, "The Activation of Platinum Electrodes by Preoxidation," *Bulletin of the Chemical Society of Japan*, vol. 36, p. 53, 1963.

[64] D. Kiuchi, H. Matsushima, Y. Fukunaka, and K. Kuribayashi, "Ohmic Resistance Measurement of Bubble Froth Layer in Water Electrolysis under Microgravity," *Journal of The Electrochemical Society*, vol. 153, no. 8, pp. E138–E143, 2006.

[65] H. Matsushima, T. Iida, and Y. Fukunaka, "Observation of bubble layer formed on hydrogen and oxygen gas-evolving electrode in a magnetic field," *Journal of Solid State Electrochemistry*, vol. 16, no. 2, pp. 617–623, 2012.

[66] B. M. Jovic, U. Lacnjevac, V. D. Jovic, and N. V. Krstajic, "Kinetics of the oxygen evolution reaction on NiSn electrodes in alkaline solutions," *Journal of Electroanalytical Chemistry*, vol. 754, pp. 100–108, 2015.

[67] A. C. Dias, M. J. Pereira, L. Brandao, P. Araujo, and A. Mendes, "Characterization of the Chlor-Alkali Membrane Process by EIS," *Journal of The Electrochemical Society*, vol. 157, no. 5, p. E75, 2010.

[68] A. M. Bond, D. Elton, S. X. Guo, G. F. Kennedy, E. Mashkina, A. N. Simonov, and J. Zhang, "An integrated instrumental and theoretical approach to quantitative electrode kinetic studies based on large amplitude Fourier transformed a.c. voltammetry: A mini review," *Electrochemistry Communications*, vol. 57, pp. 78–83, 2015.

[69] A. Bond, N. Duffy, S. Guo, J. Zhang, and D. Elton, "Changing the Look of Voltammetry," *Analytical Chemistry*, vol. 77, pp. 186A–195A, 2005.

[70] A. H. Caldwell, E. Lai, A. J. Gmitter, and A. Allanore, "Influence of mass transfer and electrolyte composition on anodic oxygen evolution in molten oxides," *Electrochimica Acta*, vol. 219, pp. 178–186, 2016.

Chapter 2

Hypothesis

The goal of electrochemical engineering is to achieve in a quantitative way an optimal cell design.

-Norbert Ibl

The need to discover high temperature materials that are capable of meeting both sustainability and productivity goals in the context of metal production was identified in the previous chapter. Electrolytic production of metals from their native ore was identified as a promising technology to meet these goals, provided that a suitable electrolyte material exist in which to perform the electrolysis. Molten sulfide electrolytes were suggested as a potential class of materials to fulfill the requirements (kinetic, thermodynamic, and transport) outlined in Section 1.2 for such an electrolyte. Electrodeposition of Fe, Cu, Mo, and Re metals has been successfully demonstrated [1, 2] in molten sulfide electrolytes, though the details of the underlying electrochemistry are limited. Specifically, knowledge of the anodic reaction,

$$2S^{2-} \rightarrow S_{2(g)} + 4e^{-} \tag{2.1}$$

is lacking. Irrespective of the cathodic metal deposition reaction, the complementary anodic reaction is sulfur gas evolution and thus understanding the chemistry of sulfur and the role of the supporting molten sulfide electrolyte in enabling electrolytic sulfur evolution is critical to engineering an optimal cell design. Sulfur and sulfides are

critical to a variety of fields including but not limited to geology, glass making, and metallurgy, all of which could greatly benefit from a deeper understanding of sulfur chemistry in molten sulfides. Gas evolution pervades a large number of sectors in the electrochemical industry. Low temperature (<100°C) electrolysis systems are by far the most extensively studied. [3–8]. To date, there are very few industrial electrochemical processes that operate in high temperature (molten) concentrated electrolytes. The best studied of course is the Hall Héroult process for smelting aluminum metal.[9] The chemical interaction of evolving gases in molten electrolytes is expected to be different from its aqueous counterpart. For instance, the solubility of chlorine gas in molten halide mixtures increases with temperature [10] in stark contrast to low temperature aqueous electrolytes which universally show a decrease in solubility with temperature. To optimize removal of anodic gas product requires knowledge of gas solubility in the electrolyte of choice as well as the active modes of mass transport away from the anode surface. At the onset of this study, both of these quantities were unknown in the case of sulfur evolution in molten sulfide electrolytes utilized for copper electrowinning.

2.1 Hypothesis

Molten sulfide electrolytes, like molten oxide and molten salt electrolytes, are concentrated ionic systems. The concentration of electroactive anions such as S^{2-} in pure molten metal sulfides is on the order of 10^1-10^2M. Thus during electrolysis, the surface concentration of these anions should differ negligibly from the bulk concentration.

Measurement of the anodic mass transfer potential allows for the determination of select hydrodynamic and thermodynamic properties of concentrated, high temperature electrolytes during electrolytic gas evolution. Due to the high temperature nature of the melts, charge transfer resistance will remain negligible even at relatively high current densities, thereby facilitating the measurement of the mass transfer overpotential. The entirety of the anodic overpotential can be attributed to an increase in the concentration of dissolved gas at the anode surface because the concentration

of precursor anions is so high that the surface concentration differs negligibly from that in the bulk.

2.2 Verification of hypothesis

This hypothesis will necessarily be tested with a range of materials. ACV, CI, and EIS techniques have all been utilized to varying extents in low temperature, aqueous-based electrolytes. The oxygen evolution reaction (OER) in room temperature aqueous electrolytes is well studied and known to be kinetically sluggish [11], thus charge transfer overpotential is expected to influence the overall overpotential measured. Critical to the determination of charge transfer overpotential is knowledge of key kinetic parameters, namely the exchange current density, j_0 and transfer coefficient, α. Plentiful data exist regarding the activities [12] of relevant species in solution and the solubility of oxygen gas in salt solutions is well documented.[13] Additionally, researchers have also measured supersaturation of O_2 at anodes using separate techniques from the ones proposed in this work which allows verification of this work's measured values of O_2 supersaturation [4, 7, 14]. Molten chlorides represent an intermediate case both in terms of temperature as well as amount of reported property data. Several studies have shown that charge transfer overpotential in simple alkali chloride mixtures is negligible, which allows one to study the ohmic and mass transfer overpotentials free of kinetic effects. Chlorine evolution at a glassy carbon electrode in a melt of lithium chloride, potassium chloride, and cesium chloride at ~350°C was studied. Having established that the proposed suite of electrochemical techniques can sufficiently described the previous two systems, the approach will be extended to sulfur evolution in a molten sulfide electrolyte.

2.3 Materials and methods

2.3.1 OER

Due to its relevance as an electrolyte for water splitting and resulting well characterized properties, aqueous potassium hydroxide solutions of varying ionic strength were used to study OER. The anode of choice was nickel which has been shown to be dimensionally stable towards OER in alkaline electrolyte. Though not dilute by most standards for electrochemical methods, concentrations of 0.36M and 3.6M KOH were used to determine if mass transfer limitations existed for hydroxide ions which would impact the total anodic mass transfer potential.

2.3.2 CER

Simple chloride salt mixtures (those free of transition metal or organic cation species) have been shown to exhibit exceptionally low overpotential for chlorine evolution.[15, 16] This is likely due to the lack of formation of electrochemically active complexes. Cl^- has been shown to be the predominant anion species in mixtures of alkali chlorides. [17] An eutectic mixture of lithium, potassium, and cesium chlorides was selected for study due to its low melting point (265°C) allowing visual observation of the anode during chlorine evolution through a quartz beaker and quartz window in a resistive heating furnace.

2.3.3 SER

Although most transition metal sulfides are molten semiconductors [18], researchers have found that sufficient dilution in alkali, alkaline earth, and/or rare earth sulfides inhibits the electronic conductivity of such melts to an acceptably low value to allow faradaic phenomena to dictate the current behavior.[1, 2] This effect has been observed with Cu, Fe, Mo, Re, and mixtures of these metal sulfides dissolved in a supporting electrolyte of BaS and/or BaS-La_2S_3. To limit any possible complications arising from the cathode reaction, cuprous sulfide was selected as the electroactive

component dissolved in supporting electrolyte because the reduced product is molten at relatively low temperature (1084°C) and the magnitude of mixed cationic valency was the lowest. Thus mixtures of Cu_2S-BaS-La_2S_3 were selected for study of the anodic sulfur evolution reaction. Due to the high temperature nature of this melt (T>1200°C), charge transfer overpotential was suspected to be negligible.

2.3.4 Electrochemical techniques

Alternating current voltammetry (ACV) provides a sensitive tool to observe faradaic phenomena.[19–22] The higher order harmonic responses of the current give insight into the faradaic reactions being observed. A preliminary survey of OER, CER, and SER utilizing ACV can help establish the similarity of current potential behavior between the three cases, in particular verifying that gas evolution is the faradaic reaction occurring, and not some undesired reaction such as impurity oxidation. Application of such techniques has already been demonstrated for molten sulfide electrolytes [1], molten salts [23], and molten oxides.[23] Having established faradaic similarity via ACV, current interrupt (CI) and electrochemical impedance spectroscopy (EIS) will be employed to further study the anodic reaction in the potential window of gas evolution. CI was successfully utilized to study the ohmic and mass transfer overpotentials established during the hydrogen evolution reaction (HER) in both aqueous sulfuric acid and potassium hydroxide solutions.[24–26] While these works did not address the charge transfer overpotential, it can be assumed that for HER, with its large exchange current density, the kinetics of charge transfer were sufficiently fast to allow the disregard of charge transfer overpotential. Ultimately, the steady state potential achieved during the current interrupt measurement provides the total overpotential ($\eta_{iR}+\eta_{ct}+\eta_{mt}$). EIS offers a complementary approach to the overpotential measurement and allows for the separation of solution resistance and charge transfer resistance. These resistances can be converted to overpotentials via Ohm's law and the Butler-Volmer equation, respectively. The remaining overpotential, deemed mass transfer overpotential can provide key insight into the hydrodynamic and thermodynamics of the evolving gases.

2.4 Summary

The need to determine hydrodynamic and thermodynamic properties of molten electrolytes has been identified. In particular, these properties in the context of anodic gas evolution were argued as the most pertinent in engineering an optimal electrowinning cell. It was hypothesized that measurement of mass transfer overpotentials at gas evolving anodes can provide insight into the (super)solubility of the evolving gas and the resulting mass transfer conditions. It was further hypothesized that sulfur evolution in molten sulfides is unhindered by charge transfer kinetics and that the mass transfer limitations at the anode arise from the removal of gaseous sulfur and not the transport of sulfide anions to the electrode surface. This hypothesis was tested in aqueous KOH and eutectic LiCl-KCl-CsCl to establish validity of the electrochemical methods before expanding these methods to the study of sulfur evolution in electrolytes consisting of Cu_2S-BaS-La_2S_3.

References

[1] S. Sokhanvaran, S.-K. Lee, G. Lambotte, and A. Allanore, "Electrochemistry of Molten Sulfides: Copper Extraction from BaS-Cu2S," *Journal of The Electrochemical Society*, vol. 163, no. 3, pp. D115–D120, 2016.

[2] S. K. Sahu, B. Chmielowiec, and A. Allanore, "Electrolytic Extraction of Copper , Molybdenum and Rhenium from Molten Sulfide Electrolyte," *Electrochimica Acta*, no. 243, pp. 382–389, 2017.

[3] W. Botter and O. Teschke, "A Method for Measuring Ohmic Resistance of Solution Layers at Gas-Evolving Electrodes," *Journal of The Electrochemical Society*, vol. 138, no. 4, pp. 1028–1033, 1991.

[4] S. Shibata, "Supersaturation of oxygen in acidic solution in the vicinity of an oxygen-evolving platinum anode," *Electrochimica Acta*, vol. 23, no. 7, pp. 619–623, 1978.

[5] J. A. Leistra, "Voltage Components at Gas Evolving Electrodes," *Journal of The Electrochemical Society*, vol. 134, no. 10, pp. 2442–2446, 1987.

[6] H. Vogt, "Heat transfer in boiling and mass transfer in gas evolution at electrodes-The analogy and its limits," *International Journal of Heat and Mass Transfer*, vol. 59, no. 1, pp. 191–197, 2013.

[7] H. Vogt, "On the supersaturation of gas in the concentration boundary layer of gas evolving electrodes," *Electrochimica Acta*, vol. 25, no. 5, pp. 527–531, 1980.

[8] H. Vogt, "On the gas-evolution efficiency of electrodes. II - Numerical analysis," *Electrochimica Acta*, vol. 56, no. 5, pp. 2404–2410, 2011.

[9] W. Haupin and H. Kvande, "Thermodynamics of Electrochemical Reduction of Alumina," *Light Metals*, pp. 379–384, 2000.

[10] J. Lorimer, H. Clever, and C. Young, *Solubility Data Series: Gases in Molten Salts*, vol. 45. 1991.

[11] C. C. L. McCrory, S. Jung, J. C. Peters, and T. F. Jaramillo, "Benchmarking Heterogeneous Electrocatalysts for the Oxygen Evolution Reaction," *Journal of the American Chemical Society*, vol. 135, no. 45, pp. 16977–16987, 2013.

[12] J. Balej, "Water vapour partial pressures and water activities in potassium and sodium hydroxide solutions over wide concentration and temperature ranges," *International Journal of Hydrogen Energy*, vol. 10, no. 4, pp. 233–243, 1985.

[13] R. E. Davis, G. L. Horvath, and C. W. Tobias, "The Solubility and Diffusion Coefficient of Oxygen in Potassium Hydroxide Solutions," *Electrochimica Acta*, vol. 12, pp. 287–297, 1967.

[14] S. Shibata, "The Anodic Behavior of Cathodically Prepolarized Bright Platinum Electrode in Sulfuric Acid Solution," *Bulletin of the Chemical Society of Japan*, vol. 33, p. 1635, 1960.

[15] A. E. Din, "Molten salt electrolysis - I. Chlorine over-potential on carbon in LiCl-KCl eutectic," *Electrochimica Acta*, vol. 4, no. August 1960, pp. 242–250, 1961.

[16] I. G. Murgulescu, S. Sternberg, L. Medintev, and C. Mustetea, "Overvoltage and depolarization in molten AgCl, AgBr and AgI," *Electrochimica Acta*, vol. 8, no. 1-2, pp. 65–75, 1963.

[17] A.-L. Rollet and M. Salanne, "Studies of the local structures of molten metal halides," *Annual Reports Section "C" (Physical Chemistry)*, vol. 107, pp. 88–123, 2011.

[18] J. E. Enderby and A. C. Barnes, "Liquid semiconductors," *Reports on Progress in Physics*, vol. 85, pp. 85–179, 1990.

[19] D. J. Gavaghan and A. M. Bond, "A complete numerical simulation of the techniques of alternating current linear sweep and cyclic voltammetry: analysis of a reversible process by conventional and fast Fourier transform methods," *Journal of Electroanalytical Chemistry*, vol. 480, no. 1-2, pp. 133–149, 2000.

[20] S. O. Engblom, J. C. Myland, and K. B. Oldham, "Must AC Voltammetry Employ Small Signals?," *Journal of Electroanalytical Chemistry*, vol. 480, no. 1-2, pp. 120–132, 2000.

[21] A. Bond, N. Duffy, S. Guo, J. Zhang, and D. Elton, "Changing the Look of Voltammetry," *Analytical Chemistry*, vol. 77, pp. 186A–195A, 2005.

[22] A. M. Bond, D. Elton, S. X. Guo, G. F. Kennedy, E. Mashkina, A. N. Simonov, and J. Zhang, "An integrated instrumental and theoretical approach to quantitative electrode kinetic studies based on large amplitude Fourier transformed a.c. voltammetry: A mini review," *Electrochemistry Communications*, vol. 57, pp. 78–83, 2015.

[23] B. R. Nakanishi and A. Allanore, "Electrochemical study of a pendant molten alumina droplet and its application for thermodynamic property measurements

of Al-Ir," *Journal of The Electrochemical Society*, vol. 164, no. 13, pp. E460–E471, 2017.

[24] H. Matsushima, D. Kiuchi, and Y. Fukunaka, "Measurement of dissolved hydrogen supersaturation during water electrolysis in a magnetic field," *Electrochimica Acta*, vol. 54, no. 24, pp. 5858–5862, 2009.

[25] D. Kiuchi, H. Matsushima, Y. Fukunaka, and K. Kuribayashi, "Ohmic Resistance Measurement of Bubble Froth Layer in Water Electrolysis under Microgravity," *Journal of The Electrochemical Society*, vol. 153, no. 8, pp. E138–E143, 2006.

[26] H. Matsushima, T. Iida, and Y. Fukunaka, "Observation of bubble layer formed on hydrogen and oxygen gas-evolving electrode in a magnetic field," *Journal of Solid State Electrochemistry*, vol. 16, no. 2, pp. 617–623, 2012.

Chapter 3

Impact of Material Properties on Overpotential Behavior at a Gas Evolving Electrode

Electrolytic gas evolution is ubiquitous in the electrochemical industry. H_2, O_2, Cl_2, CO, and CO_2 are commonly found gas products from various electrolytic processes in both aqueous and molten electrolytes. While kinetic (charge transfer) limitations dominate the overpotential behavior in most low temperature, low current density cells, it has been acknowledged that mass transfer effects are non negligible under industrially relevant current densities.[1]. The anode effect, most commonly associated with Al electrowinning, is the extreme and sudden rise in cell voltage due to formation of a non-wetting fluorocarbon (CF_4 and C_2F_6) gaseous layer that shields the carbon anode from the electrolyte. The formation of these gases was first shown to be the result of mass transfer limitations of the electroactive oxide species, $Al_2OF_6^{2-}$ by Piontelli.[2] This chapter seeks to identify key material properties that influence the various forms of overpotential associated with electrolytic gas evolution: ohmic, charge transfer, and mass transfer. For a review of gas electrode current/potential behavior, the interested reader should consult the reviews by Vogt [3–15].

3.1 Overpotential sources during electrochemical gas evolution

Overpotential is defined as the departure in potential from equilibrium to sustain a given current density. The equilibrium (Nernst) potential for a gas evolving electrode, shown in Eq 3.2 is determined by the standard oxidation[1] potential, E^0, the number of electrons exchanged, n_e, during the oxidation of two monatomic ions, X^{2n_e-} Faraday's constant, F, the universal gas constant, R, the absolute temperature, T, and the activities, a_i, of the species involved in Eq 3.1.

$$2X_{dis}^{n_e-/2} \rightarrow X_{2(g)} + n_e e^- \tag{3.1}$$

$$E = E^0 - \frac{RT}{n_e F} \ln\left[\frac{a_{X_2}}{(a_{X^{n_e-/2}})^2}\right] \tag{3.2}$$

The thermodynamics of Eq 3.1 completely determine the Nernst potential in Eq 3.2. However, to conduct this reaction at a finite rate (current density) necessitates the introduction of irreversibilities into the process: in the context of electrochemistry, these irreversibilities are referred to as overpotentials and arise from the transport of charge (ions and electrons) and mass. The overpotentials of interest during electrochemical gas evolution are as listed in Table 3.1:

Mathematical expressions for these overpotentials will be provided below, while high-

overpotential	symbol	source
ohmic	η_{iR}	conduction of ions through an electrolyte solution of finite conductivity
charge transfer	η_{ct}	exchange of electrons at electrode/electrolyte solution interface
mass transfer	η_{mt}	gradient in activity of the electroactive species from the electrolyte solution bulk to/from the electrode surface

Table 3.1: Overpotentials manifested during electrochemical gas evolution

[1] though tabulations normally reflect the standard *reduction* potential, the gas evolution reactions in this study are oxidation reactions, thus the electrochemical equations will be written with one mole of gas phase as the product

lighting the effect of properties of the electrolyte solution on these overpotentials.

3.1.1 Ohmic overpotential

Due to finite conductivity, a gradient in electrical potential exists within the electrolyte solution to sustain current flow. For sufficiently small electrical potential gradients, Ohm's law is obeyed. That is the current density, j, is proportional to the negative of the electrical potential gradient, -$\nabla\Phi$. The proportionality factor is the solution conductivity, κ. Mathematically:

$$j = -\kappa\nabla\Phi \tag{3.3}$$

Integrating Eq 3.3 over space yields the ohmic overpotential - the excess potential difference required to flow current through the electrolyte solution. Analytical integration of Eq 3.3 is possible for the simplest electrochemical cell geometries (parallel plates or concentric cylinders electrodes, etc). Finite element solvers such as COMSOL are often utilized when the current density distribution is non-uniform.

Experimentally, the ohmic overpotential can be measured via various impedance techniques, most notable of which are the current interrupt technique and electrochemical impedance spectroscopy. These techniques, described in Chapter 4, measure an effective solution resistance, R_s, which when multiplied by the current give the ohmic overpotential, η_{iR}, as shown in Eq 3.4.

$$\eta_{iR} = iR_s \tag{3.4}$$

Eq 3.4 predicts a linear dependence of η_{iR} on current (or current density) if the effective solution resistance, R_s remains constant. However in the case of gas evolution, the ohmic overpotential has been shown to increase superlinearly with the current density. During gas evolution at an electrode, a two-phase region or bubble layer can develop where the effective conductivity of the electrolyte decreases due to the near insulating properties of gases. This phenomenon, including ways to model it were

extensively reviewed by Tobias.[16] One such way to model the conductivity of this bubble layer is to treat it as a composite region of insulating ($\kappa = 0$) spheres inside of a conductive medium, giving the well known Bruggeman Equation, shown in Eq 3.5 where κ_{eff} is the effective conductivity of the two phase region, κ_ℓ, is the liquid phase conductivity, and ϕ_g is the volume fraction of the gas in the two phase region.

$$\kappa_{eff} = \kappa_\ell (1 - \phi_g)^{3/2} \tag{3.5}$$

One can see that as ϕ_g increases, the conductivity of the bubble layer tends rapidly to zero. ϕ_g is determined by the size of bubbles generated at the electrode surface, which in turn is strongly influenced by the surface tension of the electrolyte, another key material property of the electrolyte solution.

3.1.2 Charge transfer overpotential

For kinetically sluggish reactions, particularly those at low temperature, a considerable activation barrier needs to be overcome for the reaction in Eq 3.1 to be driven in either direction. The Butler Volmer equation, provided in Eq 3.6 where j is the current density, j_0 is the exchange current density, α is the transfer coefficient, n_e is the number of electrons exchanged, F is Faraday's constant, R is the universal gas constant, T is the absolute temperature, and η_{ct} is the charge transfer overpotential, is frequently chosen to describe electrode kinetics and thus has the largest database regarding the kinetic parameters involved. For clarity, this form of the Butler Volmer equation assumes negligible mass transfer effects.

$$j = j_0 \left(\exp\left(\frac{(1-\alpha) n_e F \eta_{ct}}{RT}\right) - \exp\left(\frac{-\alpha n_e F \eta_{ct}}{RT}\right)\right) \tag{3.6}$$

Eq 3.7 shows that the charge transfer resistance, R_{ct}, can be taken as the inverse of the derivative of the current (current density, j, multiplied by area, A) with respect

to the charge transfer overpotential.

$$R_{ct} = \left(\frac{d(jA)}{d\eta_{ct}}\right)^{-1} \tag{3.7}$$

For low overpotentials, ($\eta_{ct} << \frac{RT}{(1-\alpha)n_eF}$), one can linearize Eq 3.6 with respect to η_{ct}. The resulting expression for R_ct at low overpotentials after differentiation is given in Eq 3.8:

$$R_{ct,small\ \eta_{ct}} = \frac{RT}{n_eFj_0A} \tag{3.8}$$

At high overpotentials, ($\eta_{ct} > \frac{RT}{(1-\alpha)n_eF}$), the current corresponding to the back reaction is exponentially small so one can truncate Eq 3.6 to include only the anodic or only the cathodic component to current. This corresponds to Tafel behavior. Differentiation at high overpotential yields an expression for R_{ct} at high overpotential shown in Eq 3.9.

$$R_{ct,high\ \eta_{ct}} = \frac{RT}{(1-\alpha)n_eFi} = \frac{RT}{(1-\alpha)n_eFj_0A\exp\frac{(1-\alpha)n_eF\eta_{ct}}{RT}} \tag{3.9}$$

Under intermediate charge transfer overpotentials however, no simplification of the Butler Volmer equation is possible so it is required to differentiate the entire equation as shown in Eq 3.7. Having an accurate expression for R_{ct} as a function of η_{ct} is critical to connecting the measurable quantity from EIS (the charge transfer resistance) to the corresponding overpotential.

Evaluating Eqs 3.8 and 3.9, one can see that material properties of the electrolyte solution most directly impact η_{ct} through the exchange current density, j_0. j_0 is an intrinsic measure of the kinetic facility of the reaction in a specific electrolyte solution with a specific electrode material. Following the derivation in Bard and Faulkner [17], j_0 can be expressed in terms of the intrinsic rate constant, k^0, Faraday's constant, F, the number of electrons exchanged, n_e, the bulk concentrations of the oxidized and reduced species, C_O and C_R, and the transfer coefficient, α as shown in Eq 3.10:

$$j_0 = n_eFk^0C_O^{(1-\alpha)}C_R^{\alpha} \tag{3.10}$$

Thus, an electrolyte system capable of dissolving large concentrations of the electroactive species will tend to have a large exchange current density. Additionally, the structure of the electroactive species when solvated by the supporting electrolyte can affect the value of k^0. Minimal atomic rearrangement of the reactant through the transition state to the product will result in lower activation energy barriers to conversion and will have correspondingly larger k^0 values. The electrode material also affects these kinetic considerations, but will not be treated within the scope of this work.

3.1.3 Mass transfer overpotential

For thorough reviews on mass transfer in electrochemical systems, the interested reader should see the chapters by Ibl (general systems) [18] and Vogt (gas evolving systems) [3]. Section 1.4.1 highlighted the different forms of mass transport relevant in electrochemical systems. Irrespective of the mass transport mechanisms at play, electrochemical measurements are sensitive to the conditions at the electrode surface, specifically the activity of the electroactive species. Under conditions of current flow, the surface concentrations of reactants and products will be lower and higher, respectively than those in the electrolyte bulk as required to provide a net driving force for mass transfer. The resulting overpotential due to mass transport, $\eta_{mt,i}$ of a reactant or product is shown in Eq 3.11, where R is the universal gas constant, T is the absolute temperature, n_e is the number of electrons exchanged, F is Faraday's constant, ν_i is the stoichiometric coefficient of species i, $a_{s,i}$ is the surface activity of species i, and $a_{b,i}$ is the bulk activity of species i:

$$\eta_{mt,i} = \frac{\nu_i RT}{n_e F} \ln\left(\frac{a_{s,i}}{a_{b,i}}\right) \tag{3.11}$$

The total mass transfer overpotential is the sum of the individual mass transfer overpotentials. However, for systems of concentrated electrolyte solutions like molten salts and molten sulfides, the reacting anion species, X^{m-}, is present in such large concentrations, that surface depletion has been shown to be negligible and thus the

ratio of surface to bulk activity is very close to one.[3]. Thus the only contributing source to mass transfer overpotential in these concentrated electrolyte solutions is the supersaturation of gaseous product. Fukunaka, Shibata, and others have shown that dissolved gas concentrations at hydrogen and oxygen evolving electrodes can exceed 1000x the equilibrium (saturation value).[19–22]

At the equilibrium potential the net current density (and also mass flux) is zero and the activity of chemical species dissolved in the electrolyte solution is spatially uniform. When a net current flows, transport of chemical species occurs through three mechanisms: diffusion, convection, and migration. Mass transport by migration does not occur for neutral molecules, including dissolved gases. Mass transfer by diffusion results in a gradient of concentration (activity) of the electroactive species. If this gradient in concentration results in local differences in the density of the electrolyte solution, then natural convection will develop and the fluid velocity at the electrode surface will be non-zero. Physicochemical properties of the fluid determine the extent to which natural convective mass transfer will occur. The Rayleigh number (Ra), is a single dimensionless number provided that is most descriptive of the fluid conditions at the electrode surface. Eq 3.12 shows that the physical quantities that constitute the Rayleigh number are: the gravitational constant, g, a characteristic length scaled to the system size, L, the fluid density, ρ_ℓ, the concentration of chemical species in flux at the electrode surface and in the fluid bulk, C_s and C_b respectively, the dynamic viscosity of the fluid, η_ℓ and the diffusivity of species driving the difference in density, D.

$$Ra = \frac{\rho_\ell g\left(\frac{d\rho_\ell}{dC}\right)(C_b - C_s)}{\eta_\ell D} \tag{3.12}$$

The Ra number in essence reflects the ratio of buoyancy forces to viscous forces at the electrode surface. The larger the Ra number, the faster the rate of natural convection within the fluid. Typically, a transition from laminar fluid flow to turbulent fluid flow occurs at values of Ra>10^{14}. The chemical engineering literature has developed extensive correlations of the mass transfer Sherwood number, Sh_m that are based off the Ra number. These correlations typically take the form below where h_m is the

mass transfer coefficient, L is the length scale characteristic of the system, D is the diffusivity of the chemical species in the fluid, and n_1 and n_2 are fitted constants:

$$Sh_m = \frac{h_m L}{D} = n_1 Ra^{n_2} \tag{3.13}$$

References

[1] C. C. L. McCrory, S. Jung, J. C. Peters, and T. F. Jaramillo, "Benchmarking Heterogeneous Electrocatalysts for the Oxygen Evolution Reaction," *Journal of the American Chemical Society*, vol. 135, no. 45, pp. 16977–16987, 2013.

[2] R. Piontelli, B. Mazza, and P. Pedeferri, "Ricerche sui fenomeni anodici nelle celle per alluminio," *Metallurgia Italiana*, vol. 57, no. 2, pp. 51–69, 1965.

[3] H. Vogt, *Comprehensive Treatise of Electrochemistry.* New York: Springer Science & Business Media, 6 ed., 1983.

[4] H. Vogt, "Heat transfer in boiling and mass transfer in gas evolution at electrodes-The analogy and its limits," *International Journal of Heat and Mass Transfer*, vol. 59, no. 1, pp. 191–197, 2013.

[5] H. Vogt and K. Stephan, "Local microprocesses at gas-evolving electrodes and their influence on mass transfer," *Electrochimica Acta*, vol. 155, pp. 348–356, 2015.

[6] H. Vogt, "On the gas-evolution efficiency of electrodes. I - Theoretical," *Electrochimica Acta*, vol. 56, no. 3, pp. 1409–1416, 2011.

[7] H. Vogt, "On the gas-evolution efficiency of electrodes. II - Numerical analysis," *Electrochimica Acta*, vol. 56, no. 5, pp. 2404–2410, 2011.

[8] H. Vogt, "On the supersaturation of gas in the concentration boundary layer of gas evolving electrodes," *Electrochimica Acta*, vol. 25, no. 5, pp. 527–531, 1980.

[9] H. Vogt, "On the various types of uncontrolled potential increase in electrochemical reactors - The anode effect," *Electrochimica Acta*, vol. 87, pp. 611–618, 2013.

[10] H. Vogt, "Single-phase free convective mass transfer in electrochemical reactors," *The Canadian Journal of Chemical Engineering*, vol. 94, no. 2, pp. 368–373, 2016.

[11] H. Vogt, "The actual current density of gas-evolving electrodes - Notes on the bubble coverage," *Electrochimica Acta*, vol. 78, pp. 183–187, 2012.

[12] H. Vogt and R. J. Balzer, "The bubble coverage of gas-evolving electrodes in stagnant electrolytes," *Electrochimica Acta*, vol. 50, no. 10, pp. 2073–2079, 2005.

[13] H. Vogt and J. Thonstad, "The Diversity and Causes of Current-Potential Behaviour at Gas-Evolving Electrodes," *Electrochimica Acta*, vol. 250, pp. 393–398, 2017.

[14] H. Vogt, "The Quantities Affecting the Bubble Coverage of Gas-Evolving Electrodes," *Electrochimica Acta*, vol. 235, pp. 495–499, 2017.

[15] H. Vogt, "The rate of gas evolution of electrodes-I. An estimate of the efficiency of gas evolution from the supersaturation of electrolyte adjacent to a gas-evolving electrode," *Electrochimica Acta*, vol. 29, no. 2, pp. 167–173, 1984.

[16] R. E. Meredith and C. W. Tobias, "Conduction in heterogeneous systems," *Advances in Electrochemistry and Electrochemical Engineering*, vol. 2, pp. 15–47, 1962.

[17] L. R. Bard, Allen J.; Faulkner, *Fundamentals and Applications Fundamentals and Applications*. 2002.

[18] N. Ibl, "Fundamentals of Transport Phenomena in Electrolytic Systems," in *Comprehensive Treatise of Electrochemistry*, pp. 1–63, 1983.

[19] S. Shibata, "Supersolubility of hydrogen in acidic solutions in the vicinity of the hydrogen-evolving platinumm cathodes having various surface states," *Denki Kagaku*, vol. 44, no. 11, pp. 709–712, 1976.

[20] S. Shibata, "Supersaturation of oxygen in acidic solution in the vicinity of an oxygen-evolving platinum anode," *Electrochimica Acta*, vol. 23, no. 7, pp. 619–623, 1978.

[21] H. Matsushima, D. Kiuchi, Y. Fukunaka, and K. Kuribayashi, "Single bubble growth during water electrolysis under microgravity," *Electrochemistry Communications*, vol. 11, no. 8, pp. 1721–1723, 2009.

[22] H. Matsushima, T. Iida, and Y. Fukunaka, "Gas bubble evolution on transparent electrode during water electrolysis in a magnetic field," *Electrochimica Acta*, vol. 100, pp. 261–264, 2013.

Chapter 4

Electrochemical techniques to measure overpotential

This chapter briefly discusses the current interrupt and galvanostatic electrochemical impedance spectroscopy techniques have been utilized extensively to investigate the impedance of electrochemical cells.[1–4] Alternating current voltammetry will be discussed in Appendix A.

4.1 Equivalent Circuit Approach

The behavior of electrochemical cells, though intrinsically more complicated than a simple electrical circuit, can often times be adequately described in terms of simple circuit elements such as resistors, capacitors, inductors, etc. The simplest representation of an electrochemical reaction is preferred as the process of adding more and more circuit elements to fit impedance data often leads to non-physical representations. The simplest equivalent circuit that captures the behavior of many electrochemical processes is the Randle's Circuit which models a solution resistance, R_s in series with a charge transfer resistance, R_{ct} which itself is in parallel with a electrochemical double layer capacitance, C_{dl}. As transport of species to/from the electrode surface becomes limiting, an additional impedance arises and is known as Warburg impedance, Z_w. This is in series with the charge transfer resistance as both are tied to faradaic re-

actions. The equivalent circuit that will be used to interpret the impedance results herein is presented below.

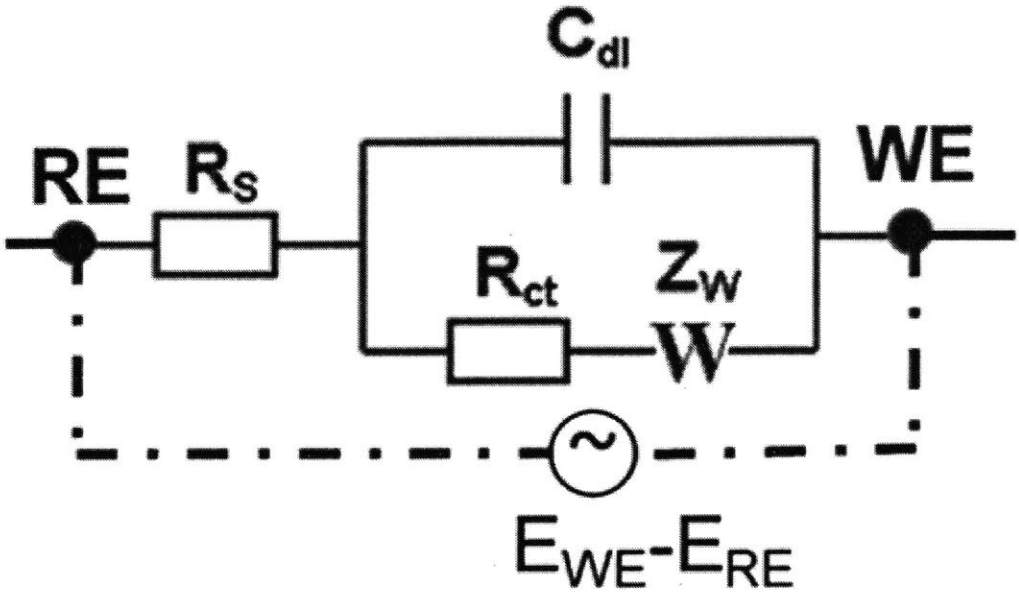

Figure 4-1: Equivalent circuit representation of the electrochemical half cell.

4.2 Current Interrupt (CI) Method

During a galvanostatic measurement, the potential between the working and reference electrodes approaches a steady state value. This potential difference is equal to the potential drop across R_s plus the potential drop across the double layer. When the current is interrupted, the potential drop across the solution resistance immediately disappears. This manifests as a discontinuity in the potential decay curve (PDC), shown in Figure 4-2. The potential across the double layer capacitor remains as the stored charge needs to discharge at a finite rate through the faradaic reaction. Thus there is a slow decay of potential back to open circuit conditions. Additionally, the

surface concentrations of the reacting species are different from those in the bulk, so the concentration gradients must also relax. The most relevant information that can be gathered from the current interrupt technique is the solution resistance and the total overpotential at a given current density.

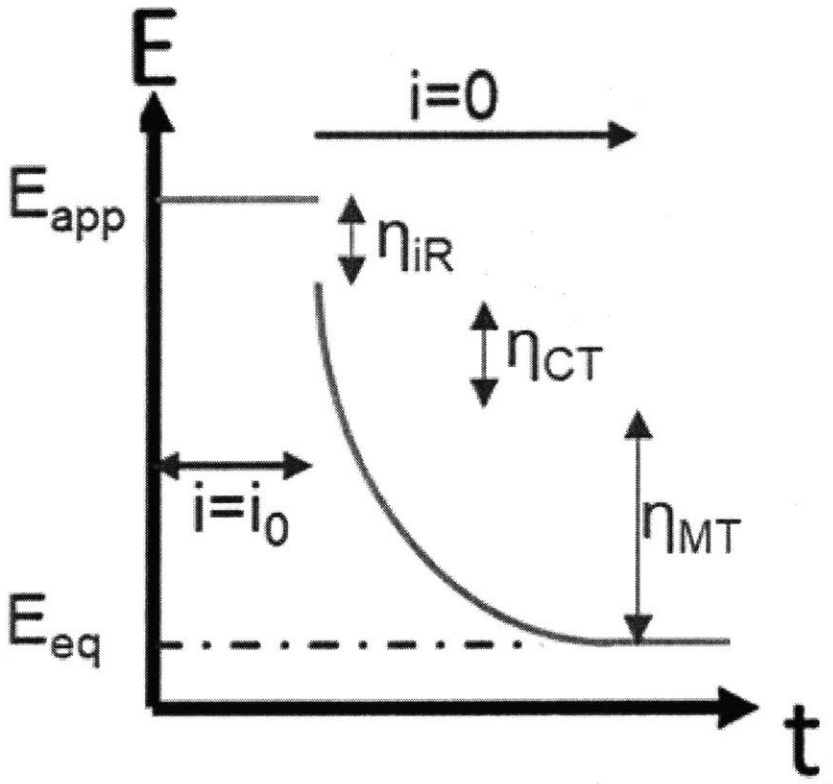

Figure 4-2: Potential Decay Curve following the interruption of current during a galvanostatic experiment.

4.3 Galvanostatic Electrochemical Impedance Spectroscopy (GEIS)

Electrochemical Impedance Spectroscopy has become the dominant method to measure the frequency response of the impedance of electrochemical cells. Looking back at Figure 4-1 , it is clear that at high frequency, the solution resistance dominates the impedance behavior as charging of the double layer offers a current short through that part of the circuit. As the frequency lowers, more and more current flows via faradaic reaction and thus R_{ct} contributes noticeably to the impedance. At the lowest frequencies, Warburg impedance dominates and the current becomes mass transport limited. These features manifest clearly in a Nyquist Plot representation of the impedance. The immediate benefit of EIS over CI is clear from such a plot. In one measurement the solution resistance and charge transfer resistance are both obtained. Relating the solution resistance and charge transfer resistance to their respective overpotentials is detailed in Sections 3.1.1- 3.1.2.

4.4 Summary

With the end goal of measuring and analyzing the mass transfer overpotential at the anode, it becomes necessary to account and correct for the ohmic and charge transfer overpotentials also present during the measurement. The CI and GEIS methods enable the selective measurement of ohmic and charge transfer overpotentials. Subtracting these overpotentials from the measured total overpotential allows for the calculation of the target mass transfer overpotential.

References

[1] H. Matsushima, D. Kiuchi, and Y. Fukunaka, "Measurement of dissolved hydrogen supersaturation during water electrolysis in a magnetic field," *Electrochimica Acta*, vol. 54, no. 24, pp. 5858–5862, 2009.

[2] D. Kiuchi, H. Matsushima, Y. Fukunaka, and K. Kuribayashi, "Ohmic Resistance Measurement of Bubble Froth Layer in Water Electrolysis under Microgravity," *Journal of The Electrochemical Society*, vol. 153, no. 8, pp. E138–E143, 2006.

[3] A. Ispas, H. Matsushima, A. Bund, and B. Bozzini, "A study of external magnetic-field effects on nickel-iron alloy electrodeposition, based on linear and non-linear differential AC electrochemical response measurements," *Journal of Electroanalytical Chemistry*, vol. 651, no. 2, pp. 197–203, 2011.

[4] A. C. Dias, M. J. Pereira, L. Brandao, P. Araujo, and A. Mendes, "Characterization of the Chlor-Alkali Membrane Process by EIS," *Journal of The Electrochemical Society*, vol. 157, no. 5, p. E75, 2010.

Chapter 5

Electrochemical Study of Oxygen Evolution in $KOH_{(aq)}$

Water electrolysis as a means to produce carbon-free fuel was first accomplished using a battery in 1800 by Nicholson and Carlisle [1] with the first industrial demonstration performed by Dmitry Lachinov in 1888. Since then, much research effort has gone into studying both the the cathodic and anodic half reactions. Incidentally, there is a wealth of information regarding the thermodynamic (decomposition and standard reduction potentials) and hydrodynamic properties (density, viscosity, surface tension, etc) of water electrolysis systems. Alkaline electrolysis, in particular has received much attention since the 1960's due to the ability of non-noble metals to catalyze the gas evolution reactions. Having such a wealth of knowledge regarding *oxygen chemistry* in alkaline electrolytes is key to understanding why and to what degree overpotential losses can develop during the oxygen evolution reaction.

5.1 Background

OER has been the interest of countless research studies [2–7] with reviews of recent developments by [8, 9], and as such, provides an excellent reference case to test the hypothesis of this work. OER in aqueous potassium hydroxide solutions in particular has been well characterized in terms of the hydrodynamic properties and thermody-

namic properties [6, 10–14]. The current interrupt technique has been applied in the literature to simple redox reactions that limited the contributions of other sources of overpotential. Hydrogen evolution at platinum electrodes also satisfies the criterion of facile charge transfer kinetics thus allowing previous researchers to apply the current interrupt technique to measure changes in solution resistance and supersaturation of hydrogen gas as a function of current density [15, 16]. We want to show that these techniques still probe the same physics in high temperature electrolytes and to facilitate signal interpretation in the higher temperature, concentrated electrolytes. Oxygen evolution is good first point of departure from the previously studied systems because its thermodynamics (gas solubility) are well understood as are the hydrodynamic properties of many aqueous based electrolytes, particularly alkaline electrolytes. The CRC handbook of Chemistry and Physics provides electrical conductivity as a function of KOH concentration [17]. Kinetic parameters relevant to electron transfer are given by McCrory [18]. Fukunaka and co-workers measured supersaturation values for oxygen production.[19, 20] Given that OER in this study was carried out at room temperature, it was expected that ohmic, charge transfer, and mass transfer overpotentials existed. Critical to separating these sources of inefficiency was knowledge of the charge transfer kinetics of hydroxide oxidation at nickel anodes. The review by McCrory [18] and the references contained within were instrumental to this effort.

5.2 Experimental

5.2.1 Materials and Equipment

0.36M and 3.6M KOH (UGR grade, Kanto Chemicals) solutions were prepared with 18MΩ-cm water and purged with oxygen (Industrial Grade, Airgas) prior to measurements. The electrochemical container was made of laser-cut polymethylmethacrolate(PMMA) which provided a transparent vessel to observe the electrolysis without the concern of ion exchange with a glass walled container. The working electrode was

a nickel plate (1cm x 1cm x 0.3cm, 99.95% pure, Nilaco Corp). The counter electrode was also a nickel plate (3cm x 1cm x 0.3cm, 99.95% pure, Nilaco Corp). The reference electrode was a nickel wire (1mm diameter, Alfa Aesar, 99.99% pure). Initial current interrupt measurements were made with a HZ-7000 potentiostat (Hokuto Denko). Subsequent CI and EIS measurements were made with a Reference 3000 potentiostat (Gamry). For ACV measurements, a Reference 3000 potentiostat (Gamry) was used in conjunction with an arbitrary waveform generator (HP 3325A) and current/voltage data were recorded at high frequency by a data acquisition module (Data Translation DT9837B).

5.2.2 Electrochemical Methods

A three electrode cell was fabricated using laser-cut acrylic that was epoxied together to give a rectangular cell volume of 13mm (W) x 50mm (L) x 300mm (H). The working and counter Ni electrodes were soldered to copper wire which acted as the electrode leads. The solder joint, back and sides of the Ni electrodes, and the copper wires were insulated with epoxy. The reference electrode was sheathed in heat shrink Teflon and position 5mm from the center of the working electrode. To mitigate the spreading of hydrogen gas bubbles from the counter electrode, a Ni mesh was positioned 1cm away from the counter electrode to trap the hydrogen bubbles. The electrochemical cell is shown in Figure 5-1. For the ACV measurements, a standard 100mL round bottom flask with ports for working, reference, and counter electrodes, as well as an inlet/outlet for oxygen purge gas was used. A Ni mesh was used as counter electrode. CI measurements were conducted at (logarithmically spaced) current densities of 1, 2.15, 4.64, 10, 21.5, 46.4, 100, and 215mA/cm^2. Galvanostatic EIS was performed at the same fixed direct current density as the CI measurements while sweeping the AC perturbation from 100kHz to 1Hz for current densities above 2.15mA/cm^2 and 100kHz to 0.1Hz for current densities of 1 to 2.15mA/cm^2. The amplitude of perturbation was 0.1mA RMS for direct currents of 1-4.64mA/cm^2 and 1mA RMS for direct currents of 10-215mA/cm^2.

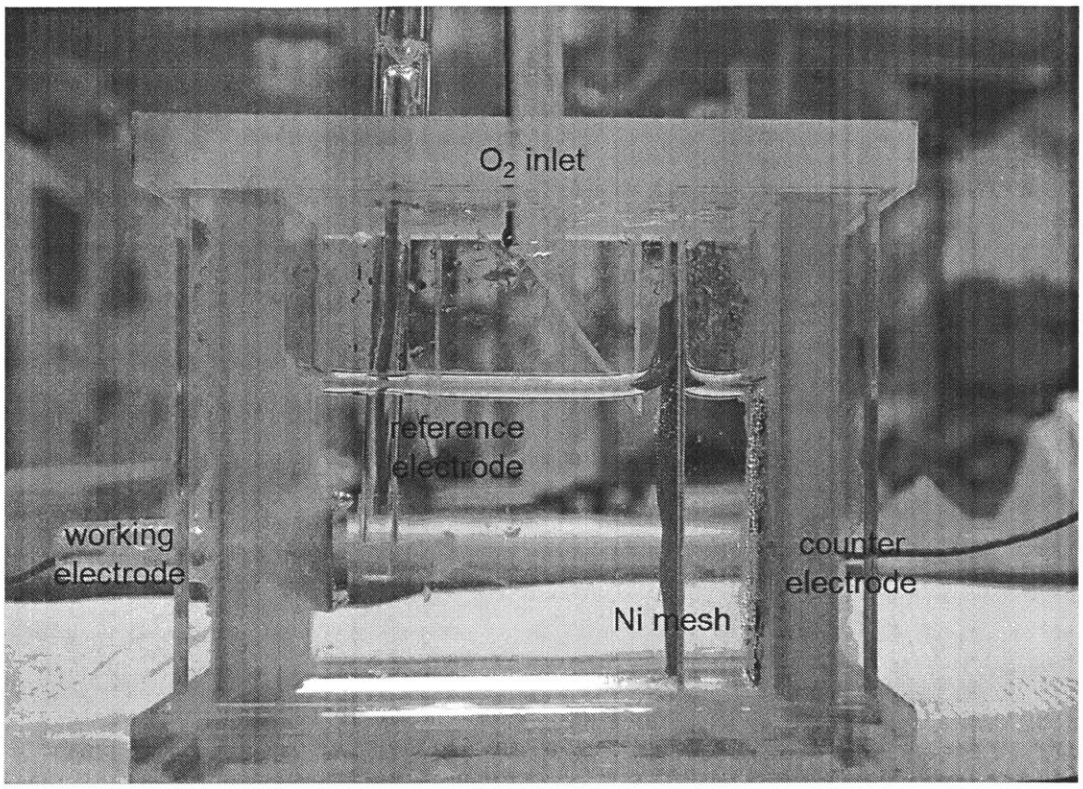

Figure 5-1: Electrochemical cell used in OER investigation. For dimensions, see text.

5.3 Results and Discussion

5.3.1 Impedance Measurements of OER at a Ni Anode

Representative Nyquist plots are presented in Figure 5-2 as parametric functions of current density. Key features are the high and low frequency real impedance intercepts which directly give the solution resistance and charge transfer resistance. Of note is the increasing nature of the high frequency intercept which indicates that the solution resistance increases as the current density increases. This has been attributed by many researchers to the development of a gaseous layer in front of the electrode surface which limits the current path, thereby increasing the effective resistance through which the ionic current must flow. In terms of effective medium theory (EMT), the gas bubbles which have exceedingly negligible electrical conductivity act as insulating spheres within a conductive medium (the electrolyte solution), thereby decreasing

the effective conductivity of the bubble layer. The Bruggeman equation, provided in Eq 5.1, has been applied to estimate the gas void fraction, ϵ, within the bubble layer next to the electrode surface utilizing the measured solution resistivities with (ρ_b) and without (ρ_0 bubble generation.

$$\epsilon = 1 - (\frac{\rho_b}{\rho_0})^{1.5} \tag{5.1}$$

Additionally, the low frequency intercept decreases with current density which is expected because the current density has an exponential dependence on charge transfer overpotential and thus at higher current densities, the slope is greater. Figure 5-3

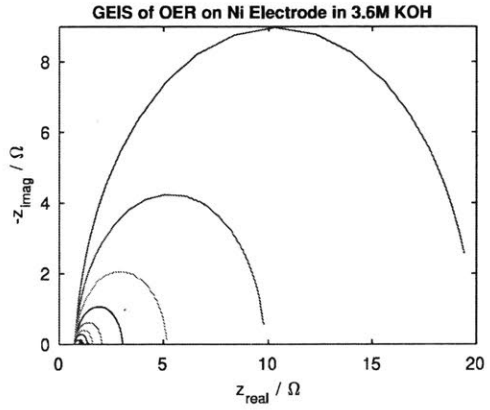

Figure 5-2: Nyquist results for OER on Ni working electrode. The semicircular curves shrink as the DC current density is increased from 1mA/cm^2 to 215mA/cm^2.

shows how the solution resistance increases as a function of current density for both 3.6M KOH and 0.36M KOH. The increase in R_s is larger for the 0.36M case compared to the 3.6M case. The conductivity of 3.6M KOH is only ~7.2x that of 0.36M KOH. Correcting for this difference in conductivity cannot explain the entire difference in solution resistance observed between the two cases. Matsushima and coworkers [11] observed similar behavior for hydrogen evolution at platinum electrodes. If nucleation were to occur homogeneously, smaller bubbles would be expected to form with a decrease in surface tension which runs contrary to this finding- the surface tension of 0.36M KOH is 72.7mN/m while that of 3.6M KOH is 83.0mN/m. Thus poorer wetting of the electrode by the electrolyte and or bubble coalescence are possible

causes for the increased solution resistance.

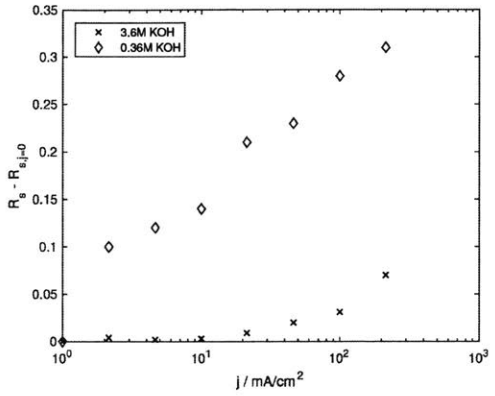

Figure 5-3: Increase in measured solution resistance as bubble evolution rate (current density) increases.

5.3.2 Overpotentials

Utilizing the low and high frequency intercepts from the Nyquist plots shown in Figure 5-2, the measured ohmic and charge transfer overpotentials are plotted in Figures 5-4 and 5-5 The difference between the total overpotential (measured during

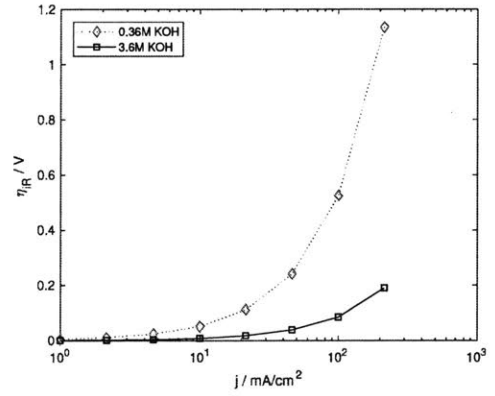

Figure 5-4: Ohmic Overpotential for OER in KOH solutions

5 minutes of galvanostatic electrolysis prior to EIS) and the sum of the ohmic and charge transfer overpotentials is attributed to mass transfer overpotential arising from surface depletion of OH^- ions and surface accumulation of $O_{2(aq)}$. The mass transfer

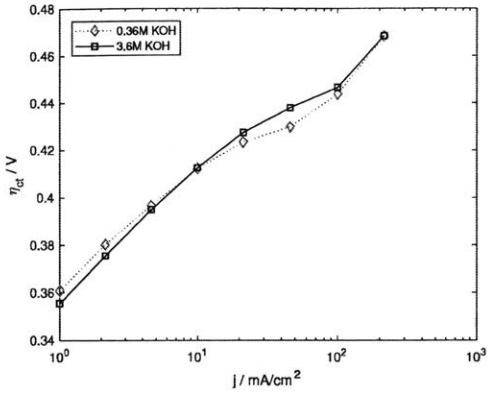

Figure 5-5: Charge Transfer Overpotential for OER in KOH solutions

overpotential is plotted in Figure 5-6. As expected, for low current densities, diffusion and/or natural convection can adequately transport reactants to and products from the electrode surface without the surface concentrations deviating from their bulk values appreciably. However, as the current density approaches and exceeds 100mA/cm^2, mass transfer overpotential rapidly increases. These current densities are extremely relevant to the industrial sector and further illustrate the need to optimize electrochemical reactor designs. Figure 5-7 compares all three overpotentials

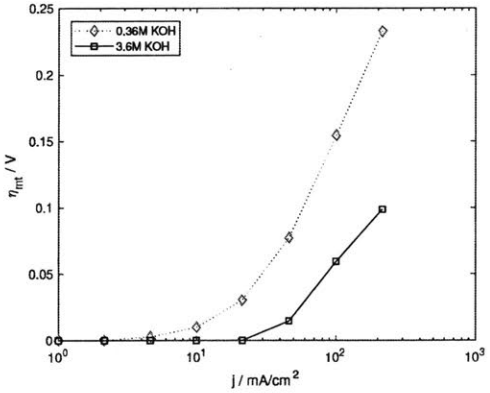

Figure 5-6: Mass Transfer Overpotential for OER in KOH solutions

side-by-side in 0.36M KOH, further highlighting that depending on the current density of interest, the physico-chemical processes that limit the behavior vary. Charge transfer kinetics dominate at low current density, but as the desired rate of reaction increases, mass transport becomes limiting. Figure 5-8 shows the estimated supersat-

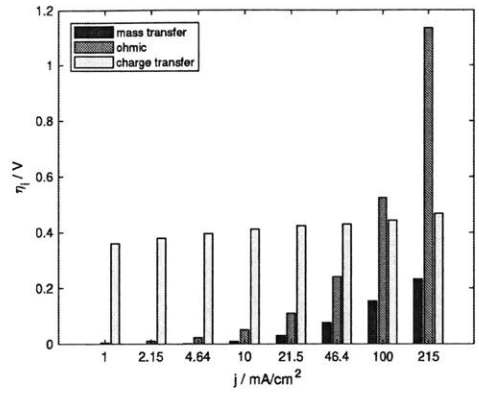

Figure 5-7: Ohmic, charge transfer, and mass transfer overpotentials for OER in 0.36M KOH

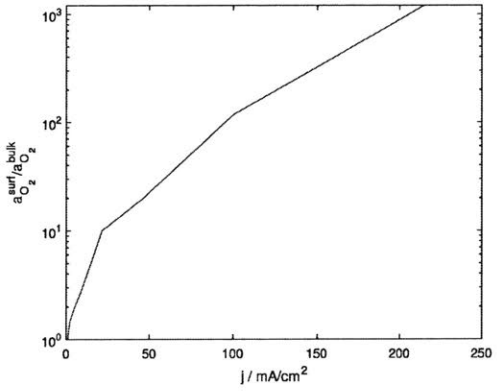

Figure 5-8: Supersaturation of O_2 gas at the anode surface

uration (activity of oxygen at the surface relative to activity in the bulk) as a function of current density during OER. The limiting value of supersaturation has not been reached, but appears to asymptotically approach a value near 2000x the equilibrium saturation value (0.14mM). This is level of supersaturation is within a factor of two of the findings by Shibata for OER.[14]

5.4 Summary

Characterization of OER on nickel plate working electrodes in 0.36M and 3.6M KOH_{aq} solutions was carried out via CI and GEIS techniques. Key findings were:

- Mass transfer overpotentials become appreciable at nominal current densities of $100 mA/cm^2$.

- Supersaturation of oxygen gas was measured to be >1000x the equilibrium value, in agreement with previous researchers measurements.

- Bubble evolution was found to increase the effective solution resistance as expected, however the relative increase was higher than expected for the lower ionic strength electrolyte.

- Charge transfer resistance was similar between the two solutions studied and dominated the total overpotential at low current densities.

References

[1] W. Nicholson, "Account of the new Electrical or Galvanic Apparatus of Sig. Alex. Volta, and Experiments performed with the same," *Journal of Natural Philosophy, Chemistry, and the Arts*, vol. 4, pp. 179–187, 1801.

[2] B. M. Jovic, U. Lacnjevac, V. D. Jovic, and N. V. Krstajic, "Kinetics of the oxygen evolution reaction on NiSn electrodes in alkaline solutions," *Journal of Electroanalytical Chemistry*, vol. 754, pp. 100–108, 2015.

[3] R. L. Doyle and M. E. G. Lyons, "An electrochemical impedance study of the oxygen evolution reaction at hydrous iron oxide in base.," *Physical Chemistry Chemical Physics*, vol. 15, no. 14, pp. 5224–37, 2013.

[4] S. M. Jasem and a. Tseung, "A Potentiostatic Pulse Study of Oxygen Evolution on Teflon-Bonded Nickel-Cobalt Oxide Electrodes," *Journal of The Electrochemical Society*, vol. 126, no. 8, p. 1353, 1979.

[5] M. E. G. Lyons and M. P. Brandon, "The significance of electrochemical impedance spectra recorded during active oxygen evolution for oxide covered Ni, Co and Fe electrodes in alkaline solution," *Journal of Electroanalytical Chemistry*, vol. 631, no. 1-2, pp. 62–70, 2009.

[6] L. J. J. Janssen, S. J. D. van Stralen, and E. Barendrecht, "Bubble behaviour on and mass transfer to an oxygen-evolving transparent nickel electrode in alkaline solution," *International Journal of Hydrogen Energy*, vol. 9, no. 10, pp. 849–853, 1984.

[7] R. F. Scarr, "The Mechanism of Oxygen Evolution on Nickel, Platinum, and Other Metals and Alloys," *Journal of The Electrochemical Society*, vol. 116, no. 11, pp. 1526–1532, 1969.

[8] N. T. Suen, S. F. Hung, Q. Quan, N. Zhang, Y. J. Xu, and H. M. Chen, "Electrocatalysis for the oxygen evolution reaction: Recent development and future perspectives," *Chemical Society Reviews*, vol. 46, no. 2, pp. 337–365, 2017.

[9] J. Mohammed-Ibrahim and S. Xiaoming, "Recent progress on earth abundant electrocatalysts for hydrogen evolution reaction (HER) in alkaline medium to achieve efficient water splitting - A review," *Journal of Energy Chemistry*, vol. 400, no. February, pp. 111–160, 2019.

[10] P. K. Weissenborn and R. J. Pugh, "Surface Tension of Aqueous Solutions of Electrolytes: Relationship with Ion Hydration, Oxygen Solubility, and Bubble Coalescence," *Journal of Colloid and Interface Science*, vol. 184, no. 2, pp. 550–563, 1996.

[11] H. Matsushima, T. Iida, and Y. Fukunaka, "Observation of bubble layer formed on hydrogen and oxygen gas-evolving electrode in a magnetic field," *Journal of Solid State Electrochemistry*, vol. 16, no. 2, pp. 617–623, 2012.

[12] L. Abdelouahed, R. Hreiz, S. Poncin, G. Valentin, and F. Lapicque, "Hydrodynamics of gas bubbles in the gap of lantern blade electrodes without forced flow of electrolyte: Experiments and CFD modelling," *Chemical Engineering Science*, vol. 111, pp. 255–265, 2014.

[13] R. E. Davis, G. L. Horvath, and C. W. Tobias, "The Solubility and Diffusion Coefficient of Oxygen in Potassium Hydroxide Solutions," *Electrochimica Acta*, vol. 12, pp. 287–297, 1967.

[14] S. Shibata, "Supersaturation of oxygen in acidic solution in the vicinity of an oxygen-evolving platinum anode," *Electrochimica Acta*, vol. 23, no. 7, pp. 619–623, 1978.

[15] H. Matsushima, D. Kiuchi, and Y. Fukunaka, "Measurement of dissolved hydrogen supersaturation during water electrolysis in a magnetic field," *Electrochimica Acta*, vol. 54, no. 24, pp. 5858–5862, 2009.

[16] T. Iida, H. Matsushima, and Y. Fukunaka, "Water Electrolysis under a Magnetic Field," *Journal of The Electrochemical Society*, vol. 154, no. 8, pp. E112–E115, 2007.

[17] R. Weast, *CRC Handbook of Chemistry and Physics, 70th Edition*, vol. 70. 1989.

[18] C. C. L. McCrory, S. Jung, J. C. Peters, and T. F. Jaramillo, "Benchmarking Heterogeneous Electrocatalysts for the Oxygen Evolution Reaction," *Journal of the American Chemical Society*, vol. 135, no. 45, pp. 16977–16987, 2013.

[19] G. Sakuma, Y. Fukunaka, and H. Matsushima, "Nucleation and growth of electrolytic gas bubbles under microgravity," *International Journal of Hydrogen Energy*, vol. 39, no. 15, pp. 7638–7645, 2014.

[20] J. Deconinck, A. Hubin, T. Nierhaus, S. V. Damme, H. V. Parys, and P. Maciel, "New model for gas evolving electrodes based on supersaturation," *Electrochemistry Communications*, vol. 11, no. 4, pp. 875–877, 2009.

Chapter 6

Electrochemical Study of Chlorine Evolution in Eutectic LiCl-KCl-CsCl

As described in the previous chapter, the combination of current interrupt and galvanostatic electrochemical impedance spectroscopy enabled the deconvolution of total overpotential into its individual components, namely ohmic, charge transfer, and mass transfer overpotentials. The values determined for the measured overpotentials agreed well with results from previous researchers, who took great care to operate under conditions where the effect of only one source of overpotential was dominant, which validates the approach taken in this work of measuring simultaneously multiple sources of overpotential. Molten salt electrolyte solutions offer a distinct chemical environment for dissolved gases as compared to aqueous KOH electrolyte solutions, namely in terms of ionic strength as well as temperature. With the end goal of characterizing sulfur evolution in molten sulfide electrolytes, the study of chlorine evolution in a molten halide electrolyte solution offers a strategic reference system in that physical and electrochemical properties are still reasonably well characterized, but also closer in nature to molten sulfides in terms of high concentration of the anion species of the dissolved gas and facilitated charge transfer kinetics due to elevated temperature.

6.1 Background

The eutectic of LiCl-KCl-CsCl has a molar composition of 57.5% LiCl - 13.3% KCl - 29.2% CsCl. This mixture has a melting point of 538K. The ionic strength based on molality is 12m. Physical and electrochemical properties were measured by Ito.[1, 2] Electrochemical studies revealed near-ideal behavior of the electrolyte solution with the measured electrochemical window being within a few millivolts of that for LiCl at an activity of 0.575. The respective cathode and anode products were indeed found to be lithium metal and chlorine gas. It has been shown that for simple alkali chloride mixtures, the electroactive anion species is Cl^- [3], thus the anticipated anodic reaction is:

$$2Cl^-_{(dis)} \rightarrow Cl_{2(g)} + 2e^- \tag{6.1}$$

Additionally, many researchers have shown negligible charge transfer overpotential for chlorine evolution in simple alkali (free of organic and transition metal cations) chloride molten salt electrolyte solutions.[4, 5] Thus the study of CER poses perhaps the simplest oxidation reaction to study in concentrated electrolyte systems. Also important is the dissolved state of the gas. Kobolov showed using electronic absorption spectroscopy of chlorine saturated alkali chloride melts that chlorine remains diatomic when dissolving into these chloride melts, rather than dissociating into Cl atoms.[6]. This matches the known behavior for O_2 in aqueous solutions.

6.2 Experimental

6.2.1 Materials and Equipment

Reagent-grade LiCl (Wako Pure Chemical Co., Ltd., 99.0%), KCl (Wako Pure Chemical Co., Ltd., 99.5%), and CsCl (Wako Pure Chemical Co., Ltd., 99.0%) were dried under vacuum for more than 24 h at 200°C. The eutectic mixture $(LiCl)_{57.5}$-$(KCl)_{13.3}$-$(CsCl)_{29.2}$ was mixed together in an ultra-dry chamber followed by melting in a resistive heating furnace inside of an argon purged glovebox. A 54mm diameter flat

bottomed closed one end quartz tube served as the crucible. The working electrode was a glassy carbon rod (4mm diameter, Tokai Carbon Co., Ltd.). The counter electrode was a Ni wire (1mm diameter, Nilaco Corp, 99.95%), and the reference electrode was a two-phase Li-Al alloy whose preparation has been described elsewhere.[7] This alloy has been shown to maintain a stable potential vs Li/Li^+ for more than 12 hours. An HZ-3000 potentiostat (Hokuto Denko) was used to perform electrochemical measurements. A small window in the side of the furnace allowed for visualization of the cell during the experiment. A picture of the electrochemical cell inside of the furnace is provided in Figure 6-1. The temperature was controlled using a type-K thermocouple that was inserted directly into the melt. A process temperature of 348.1°C +/- 0.2°C was maintained.

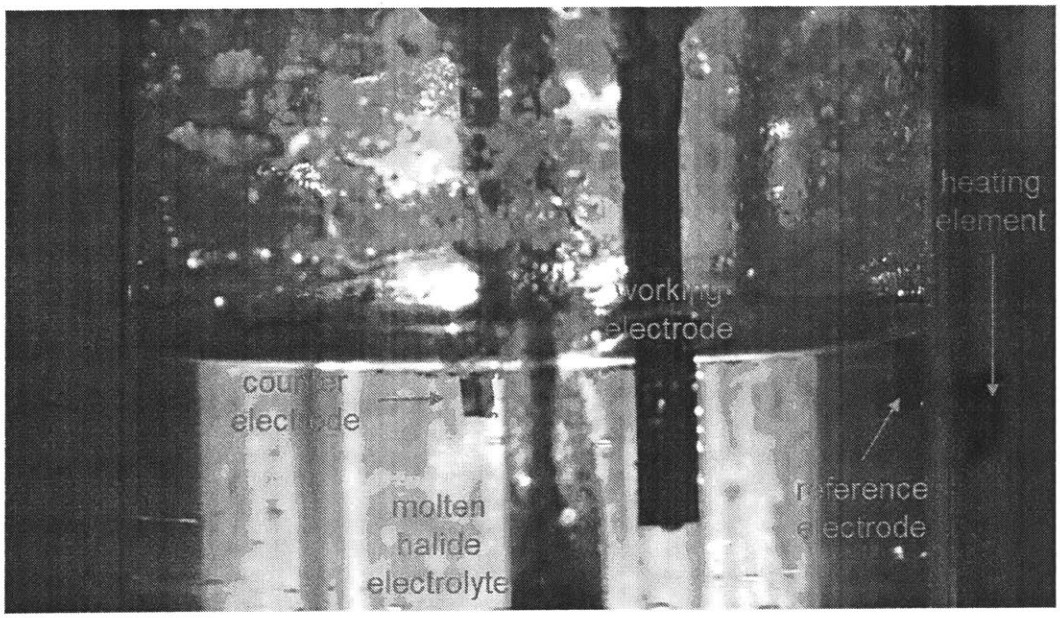

Figure 6-1: Electrochemical cell used in CER investigation. For dimensions, see text.

6.2.2 Electrochemical Methods

The electrolyte solution was saturated in chlorine by electrochemically generating Cl_2 from the anode for a period of several minutes. CI measurements were conducted at (logarithmically-spaced) current densities of 1, 2.15, 4.64, 10, 21.5, 46.4, 100, 215,

464, and 1000mA/cm^2. The current density was held fixed for 5 minutes to establish a steady-state potential and allow convection to fully develop before interrupting the current and measuring the potential decay curve. The current and potential were recorded without the use of an external DAQ at a sampling rate of 50kHz.

6.3 Results and Discussion

6.3.1 Current Interrupt

Figure 6-2 shows a typical potential decay curve (PDC) for CER at the various current densities studied. Due to parasitic capacitance in the potentiostat cables, it

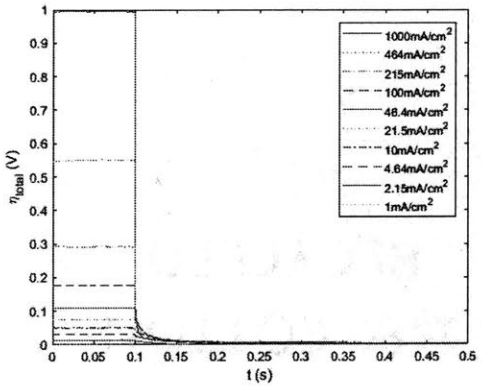

Figure 6-2: Potential decay curves for chlorine evolution in eutectic molten salt

was necessary to extrapolate the the PDC back to the time of interrupt. Linear and exponential extrapolation are the most common methods. Figure 6-3 shows graphically the method of extrapolation of the PDC when a current density of 100mA/cm^2 was interrupted. It was found that the measured value of ohmic overpotential was insensitive to the choice of linear versus exponential extrapolation. Of note is the swift decay of overpotential back to the open circuit (equilibrium) value in Figure 6-2. Video analysis of the electrode surface revealed that bubbles remained attached to the glassy carbon surface for >10s after the cessation of current. Figure 6-4 is a picture of the electrode before and after a current density of 100mA/cm^2 was interrupted. The diameter of bubbles spanned from $\sim$100μm to >1mm. The implications of this

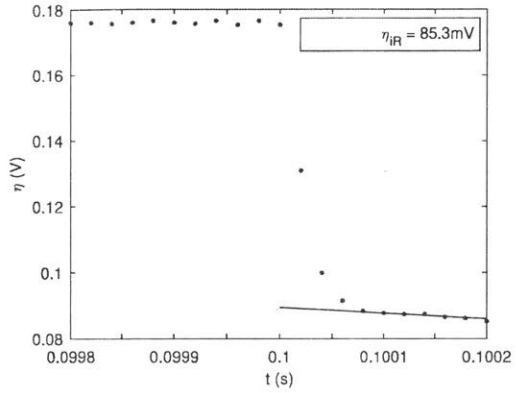

Figure 6-3: Linear extrapolation of the potential decay curves for chlorine evolution in eutectic molten salt after a current density of 100mA/cm^2 was interrupted.

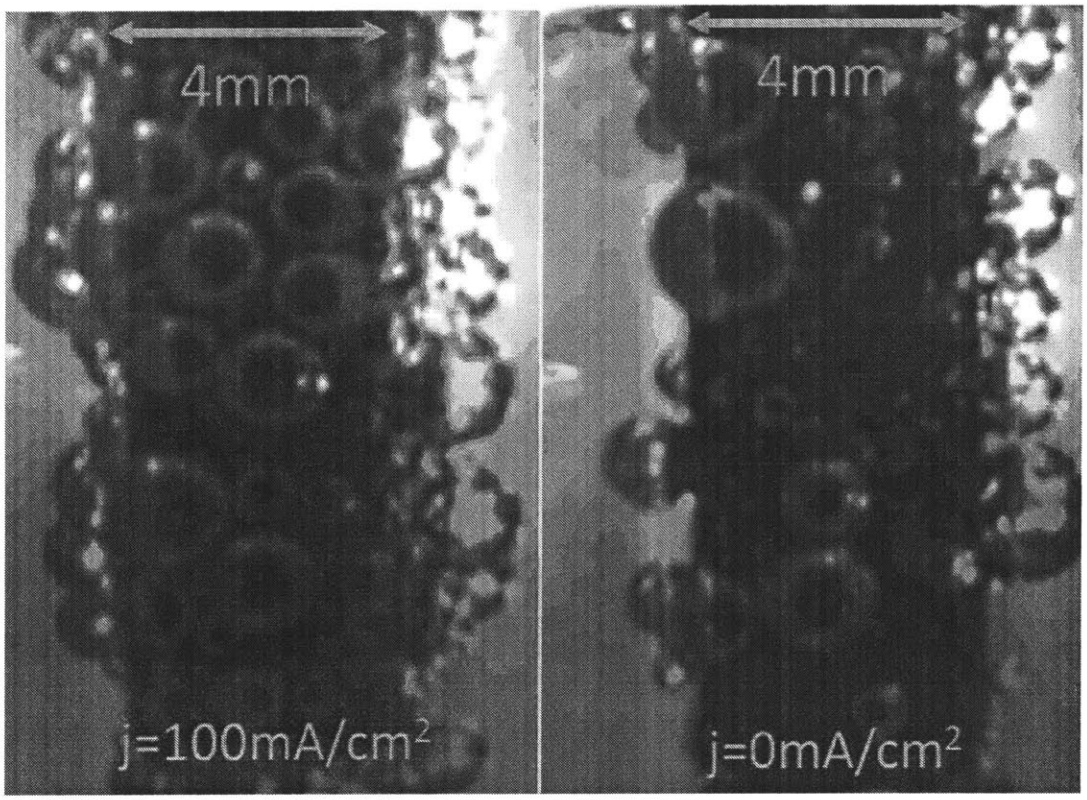

Figure 6-4: Surface layer of Cl_2 bubbles during and after galvanostatic electrolysis at 100mA/cm^2 in molten salt

observation are two-fold: the wettability of glassy carbon by the molten electrolyte is poor, resulting in gas being trapped on the surface, and there are two modes of mass

transport of $Cl_{2(dis)}$ away from the electrode after current interruption: convective transport of the dissolved gas to the bulk as well as evaporation into the gas phase present as bubbles attached to the electrode surface. This latter mode is confirmed as the radii of bubbles attached to the electrode surface grew with time after the current interruption. Figures 6-5 and 6-6 show the ohmic and mass transfer overpotentials, respectively, in the measured system. The reference electrode was positioned 3cm

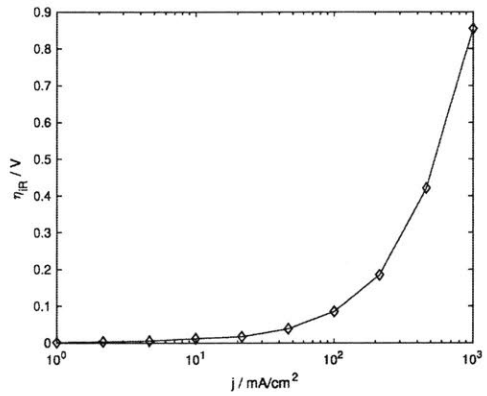

Figure 6-5: Ohmic overpotential for chlorine evolution

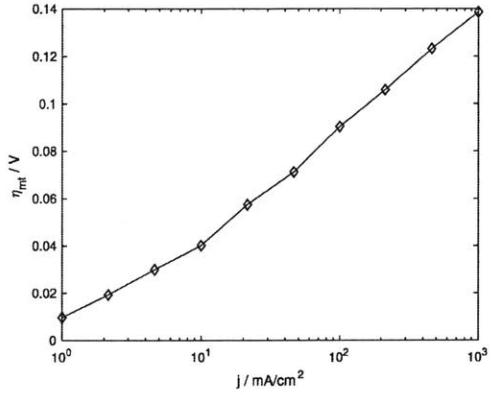

Figure 6-6: Mass Transfer overpotential for chlorine evolution

away from the working electrode, thus resulting in the substantially large ohmic overpotential. The trend in overpotential with nominal current density clearly shows the importance of solution conductivity as the ohmic overpotential grows super-linearly with current density while the mass transfer overpotential is growing roughly logarithmically with current density. The growth in solution resistance with increasing

current density has been well documented [8, 9], and attributed to a restriction in path of the current through the bubble layer. Video recordings did not allow for accurate determination of surface bubble coverage (θ), but the relative size of bubbles was not found to vary significantly with current density. It is not unexpected for θ to continue to grow with current density as shown by Vogt.[10–12].

Of interest is that despite the large current densities studied (up to 1000mA/cm^2) the supersaturation observed for Cl_2 has not yet reached an asymptotic limit, as shown in Figure 6-7. This finding indicates that the gas evolution efficiency, f_g is still less than one under these flow conditions. Lastly, knowledge of Cl_2 saturation concentration

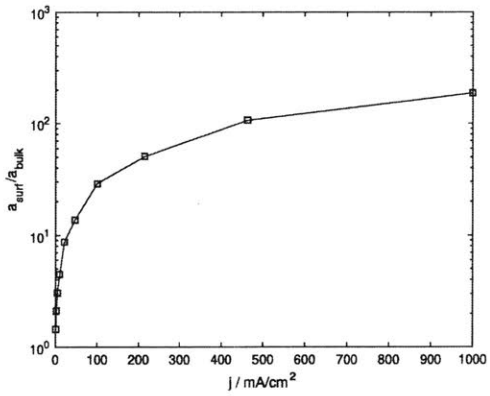

Figure 6-7: Supersaturation of Cl_2 observed in molten salt study

allows one to calculate the mass transfer coefficient to the electrode surface based on a simple equation of mass transport ($j = n_e F * n" = n_e F h_m C_b(\frac{C_s}{C_b} - 1)$). Figure 6-8 shows the variation of the mass transfer coefficient with current density. The rate of increase in the coefficient increases more rapidly with increasing current density. This is likely due to the enhanced convection by the bubble evolution rate.

6.4 Summary

Characterization of CER with a glassy carbon rod working electrode in a molten chloride electrolyte of composition $(LiCl)_{57.5}$-$(KCl)_{13.3}$-$(CsCl)_{29.3}$ at 348°C was carried out using the current interrupt technique and video recording. Key findings were:

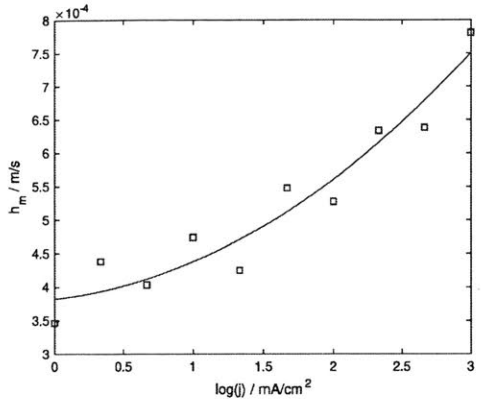

Figure 6-8: Variation of mass transfer coefficient in molten salt as Cl_2 evolution current density increases.

- The mass transfer overpotential depended linearly on the current density over the entire range studied.

- The concentration of Cl^- in this system is ~28M which is » the saturation concentration of dissolved chlorine (~1mM) which strongly suggests that all mass transfer limitations at the anode are associated with removal of the dissolved gas.

- Supersaturation of chlorine grew linearly with current density, reaching a value of >180x the equilibrium value at a current density of $1000mA/cm^2$.There appears to be an asymptotic limit to the degree of supersaturation, but it was not experimentally accessible.

- Large bubbles (>1mm) were found to stick to the electrode surface, indicating poor wettability of the melt on glassy carbon.

- The calculated mass transfer coefficient increased with current density which was corroborated with an increase velocity of the bubble layer adjacent to the electrode surface.

References

[1] T. Murakami, T. Nohira, Y. H. Ogata, and Y. Ito, "Electrochemical Window of a LiCl-KCl-CsCl Melt," *Electrochemical and Solid-State Letters*, vol. 8, no. 1, pp. E1–E3, 2004.

[2] H. Ito, Y. Hasegawa, and Y. Ito, "Densities of eutectic mixtures of molten alkali chlorides below 673 K," *Journal of Chemical and Engineering Data*, vol. 46, no. 5, pp. 1203–1205, 2001.

[3] A.-L. Rollet and M. Salanne, "Studies of the local structures of molten metal halides," *Annual Reports Section "C" (Physical Chemistry)*, vol. 107, pp. 88–123, 2011.

[4] A. E. Din, "Molten salt electrolysis - I. Chlorine over-potential on carbon in LiCl-KCl eutectic," *Electrochimica Acta*, vol. 4, no. August 1960, pp. 242–250, 1961.

[5] I. G. Murgulescu, S. Sternberg, L. Medintev, and C. Mustetea, "Overvoltage and depolarization in molten AgCl, AgBr and AgI," *Electrochimica Acta*, vol. 8, no. 1-2, pp. 65–75, 1963.

[6] A. Kolobov, V. Khokhlov, A. Potapov, and V. Kochedykov, "Chlorine solutions in molten alkali chlorides," *Zeitschrift fur Naturforschung - Section A Journal of Physical Sciences*, vol. 62, no. 3-4, pp. 205–212, 2007.

[7] T. Kasajima, T. Nishikiori, T. Nohira, and Y. Ito, "Electrochemical window and the characteristics of (α + β) Al-Li alloy reference electrode for a LiBr-KBr-CsBr eutectic melt," *Journal of the Electrochemical Society*, vol. 151, no. 11, pp. E335–E339, 2004.

[8] D. Kiuchi, H. Matsushima, Y. Fukunaka, and K. Kuribayashi, "Ohmic Resistance Measurement of Bubble Froth Layer in Water Electrolysis under Microgravity," *Journal of The Electrochemical Society*, vol. 153, no. 8, pp. E138–E143, 2006.

[9] H. Matsushima, D. Kiuchi, and Y. Fukunaka, "Measurement of dissolved hydrogen supersaturation during water electrolysis in a magnetic field," *Electrochimica Acta*, vol. 54, no. 24, pp. 5858–5862, 2009.

[10] H. Vogt and R. J. Balzer, "The bubble coverage of gas-evolving electrodes in stagnant electrolytes," *Electrochimica Acta*, vol. 50, no. 10, pp. 2073–2079, 2005.

[11] H. Vogt, "The actual current density of gas-evolving electrodes - Notes on the bubble coverage," *Electrochimica Acta*, vol. 78, pp. 183–187, 2012.

[12] H. Vogt, "The Quantities Affecting the Bubble Coverage of Gas-Evolving Electrodes," *Electrochimica Acta*, vol. 235, pp. 495–499, 2017.

Chapter 7

Electrochemical Study of Sulfur Evolution in BaS-La_2S_3-Cu_2S

Knowledge of the physicochemical and hydrodynamic properties of molten sulfide electrolytes as obtained using electrochemistry is an opportunity to test the hypothesis and to better understand chemical nature of these special solvents. The previous two chapters showed that measuring the total overpotential (via current interrupt) and the solution and charge transfer resistances via galvanostatic EIS was sufficient to separately determine the ohmic, charge transfer, and mass transfer overpotential during anodic gas evolution. Molten sulfide electrolyte solutions are considerably less-studied than the aqueous and molten salt electrolyte systems studied in the previous chapters. Molten sulfide electrolyte solutions consisting of BaS or BaS+La_2S_3 with transition metal sulfides have been shown as effective media in which to conduct Faradaic reactions. However the lack of knowledge concerning their physicochemical properties remains a challenge when envisioning large scale applications. Thus the application of the electrochemical methods demonstrated in Chapters 5 and 6 may help elucidate the role of transfer of charge (both ions and electrons) or mass (ions and neutral species) on the anodic evolution of sulfur as shown in Eq 7.1.

$$2S^{2-}_{dis} \rightarrow S_{2(g)} + 4e^{-} \tag{7.1}$$

Appendix A has the results of AC voltammetry studies to demonstrate Faradaic similarity between OER, CER, and SER.

7.1 Background

Electronic properties of binary metal sulfides span a wide range of behavior in the composition and temperature spaces. Barium sulfide is a high melting point, large band gap sulfide (MP = 2235°C [1], E_g = 3.92eV [2]). Lanthanum (III) sulfide is also a high melting point, large band gap sulfide (MP = 1977-2127°C [3], E_g = 2.73eV [4]) Cuprous sulfide, Cu_2S, is a transition metal sulfide that is a semiconductor,(MP = 1130°C , E_g = 1.3eV [5]). In fact, most of the transition metal sulfides behave as semiconducting or metallic liquids above their melting points. Despite this behavior, Sokhanvaran and coworkers at MIT showed that a molten mixture of BaS and Cu_2S could be electrolyzed to generate liquid copper metal and gaseous elemental sulfur.[6] Stinn mapped out the complete phase diagram for the BaS-Cu_2S system.[1] Interestingly, a region of liquid-liquid immiscibility exists in the high BaS region (72-92mol% BaS) of the phase diagram. Visualization of these two liquids using a thermal imaging furnace revealed that one of the liquids was shiny (metallic-like) and the other dull. Further analysis revealed that the dull component (high BaS content) was found to be ionic, rather than semiconducting in nature. This finding motivates the decision to use high BaS + La_2S_3 content electrolyte solutions for electrolysis. Sahu and the author showed that the addition of La_2S_3 as supporting electrolyte allowed for higher current efficiency for copper production.[7] Thus a mixture of BaS, La_2S_3, and Cu_2S with the mole fraction of Cu_2S =0.1 was selected in this study.

Under the operating conditions of the melt, the anticipated anodic reaction is written in Eq 7.1. The expectation that S^{2-} is the electroactive anion in solution is justified for the following reasons:

- The oxidation state of sulfur is (-2) in the precursor powders for the electrolyte melt.

- Unlike the alkali sulfides which readily form stable polysulfides (e.g. Na_2S_x, K_2S_x, x=2-5), the only stable compound of barium and sulfur at high temperature is BaS.[8]

- Formation of polysulfide (S_n^{2-}) from monatomic sulfide (S^2-) is an oxidation process. If this oxidation were to occur, another species in the electrolyte must be concurrently reduced.

- Ba^{2+} is isoelectronic with Xe, thus the divalent state is energetically favored.

- La^{3+} has an empty f subshell of electrons thus making the trivalent state by far the most stable oxidation state.[9]

- Cuprous ions can only be reduced to metallic copper, yet no metal is found after heating the electrolyte to temperature without performing electrolysis.

- Typically <1% weight loss occurs upon melting the precursor powders without noticeable condensation of volatile species anywhere in the reaction tube, thus the chemical composition does not change appreciably,

7.2 Experimental

7.2.1 Materials and Equipment

As mentioned in the background section, this study would be limited to electrolyte melts with a mole fraction of Cu_2S under 0.2. A melt with a molar composition of $(BaS)_{54}$-$(La_2S_3)_{36}$-$(Cu_2S)_{10}$ was selected for study. The powder precursors for all electrochemical experiments were BaS (Alfa Aesar, 99.7% metals basis), La_2S_3 (Strem Chemical, 99.9% metals basis), and Cu_2S (Alfa Aesar, 99.5% metals basis). Due to the hygroscopic nature of the sulfides, the sample preparation and storage was conducted inside of an argon-purged glovebox. Powders were weighed individually before being ground and thoroughly mixed together with a mortar and pestle inside of the glovebox. Premelts for experiments were similarly prepared by heating in a

graphite crucible (Beijing Great Wall Co., M2-grade purified to <50ppm ash content) in a resistive heating furnace to 1200°C before cooling back down. Mass loss was <1%.

A schematic of the electrochemical cell is shown in Figure 7-1. The working

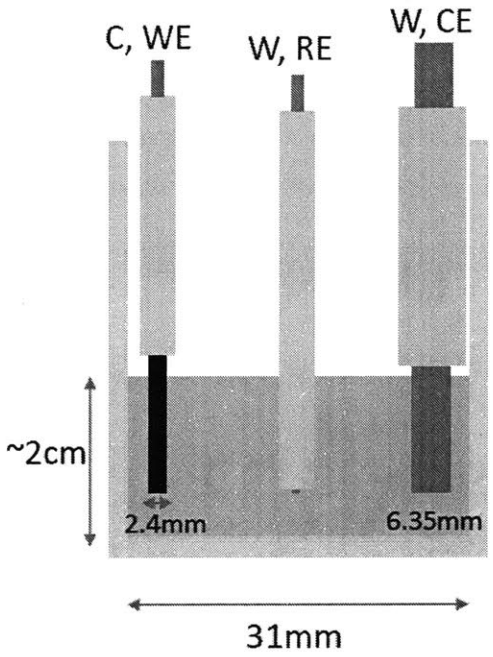

Figure 7-1: Schematic of electrochemical cell used for mass transfer investigation of SER.

electrode was a graphite rod (Alfa Aesar, 2.4mm diameter, 25mm height, 99.9995% purity). The exposed surface area was set to 1.176cm^2 and controlled by the placement of an insulating alumina sheathe. The pseudo-reference electrode was a tungsten rod (Ed Fagan Inc, 1mm diameter, 99.95% purity) that was sheathed with an alumina tube so that only the flat bottomed face was exposed. The counter electrode was a tungsten rod (Ed Fagan Inc, 6.35mm diameter, 99.95% purity) with an exposed surface area of 6.3cm^2. While the entire leads for the reference and counter electrode were tungsten, the lead for the working electrode was a molybdenum rod (Ed Fagan Inc, 1.76mm diameter, 99.95% purity). 46g of premelt were transferred to an alumina crucible (AdValue Technology, 31mm diameter, 100mm height, 99.8% Al_2O_3). The crucible was placed in the hot zone of a resistive heating furnace (Mellen Company,

SS15R-2.50X6V-1Z) and heated under argon flow to 1300°C (controlled by a Type-R thermocouple). After being held at temperature for one hour, the electrodes were lowered and allowed to thermally equilibrate for 20 minutes before commencing the experiment.

Electrochemical measurements were made with a potentiostat (Gamry, Reference 3000).

7.2.2 Electrochemical Methods

The electrolyte melt was saturated in sulfur by electrochemically generating S_2 from the anode for a period of several minutes. Current Interrupt (CI) measurements were conducted at logarithmically-spaced current densities followed immediately by galvanostatic electrochemical impedance spectroscopy (GEIS) performed at the same fixed direct current densities as the CI measurements. Table 7.1 provides the values of operating parameters utilized in this study.

direct current density (mA/cm^2)	perturbation amplitude (mA/cm^2 RMS)
1.00	0.0100
2.15	0.0215
4.64	0.0464
10.0	0.100
21.5	0.215
46.4	0.464
100	1.00
215	2.15
464	4.64
1000	10.0

Table 7.1: CI and GEIS parameters utilized during the study of SER at a graphite working electrode. The frequency range investigated was 50kHz-1Hz for all conditions.

7.3 Results and Discussion

7.3.1 Current Interrupt

Galavanostatic electrolysis at the current density range studied showed typical behavior for a gas evolving electrode: at higher current densities, the potential fluctuated around a mean value rather than achieve a true steady state value as seen in Figure 7-2. Because the data sampling rate for the current and potential was relatively low

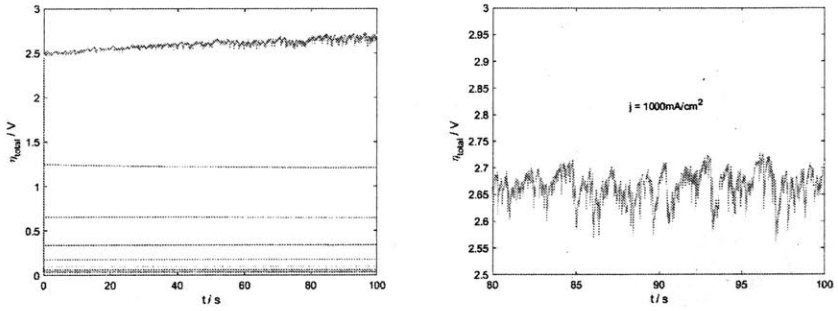

Figure 7-2: Left: Total overpotential during SER at 1300°C. Right: Potential fluctuations are observed to increase drastically at 1000mA/cm^2.

(100Hz), no effort was made to calculate the ohmic overpotential from the potential jump in the potential decay curve. Rather, the high frequency real impedance intercept of the Nyquist curve was utilized to determine the ohmic overpotential (next section).

7.3.2 Galvanostatic EIS

Each galvanostatic EIS measurement was performed immediately after the corresponding CI measurement to ensure that the hydrodynamic conditions remained fully developed. A larger perturbation current density than the aqueous case was required to reduce noise during the measurement. A typical Nyquist plot collected during this study is presented below in Figure 7-3. The key feature in all of the impedance measurements is the complete absence of a resistive charge transfer component to the Nyquist curve: a Warburg-like impedance immediately dominates the impedance

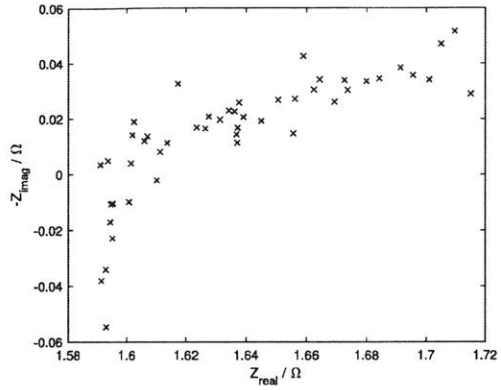

Figure 7-3: Left) Nyquist curve obtained for SER at a graphite working electrode under a direct current density of $46.4 mA/cm^2$. The frequency range investigated was 50kHz to 1Hz.

behavior at lower frequencies. This behavior is quite common in molten salts and is not unexpected given the elevated temperature of operation. Additionally, the lack of charge transfer resistance hints at the structural nature of the electroactive sulfide anion in the electrolyte melt. If it were to exist under the conditions present in the molten sulfide electrolyte, a bulky, conformationally complex polyanion such as S_8^{2-} is unlikely to have a negligible activation energy upon oxidizing to S_2. Figure 7-4 shows the FactSage predicted equilibrium composition of sulfur vapor (S_{1-8}) as a function of temperature. As expected, entropy maximization favors the smaller chain length allotropes, with the S_2 molecule being the overwhelmingly favored allotrope at temperatures $> 700°C$. Thus, analogous to free oxygen (O^{2-}) in silicate slags which also show negligible anodic charge transfer resistance [10–12], the electroactive ion in MSE appears to be S^{2-}

Using the solution resistance determined by the real impedance intercept from the GEIS Nyquist curves, shown above, and the current under which the GEIS was performed allowed the ohmic overpotential to be straightforwardly calculated and is presented in Figure 7-5. Again, the established lack of charge transfer resistance allows the remainder of overpotential to be attributed to mass transfer overpotential for SER. The corresponding overpotential is plotted in Figure 7-6. The reference electrode was positioned 2cm away from the working electrode, thus resulting in the

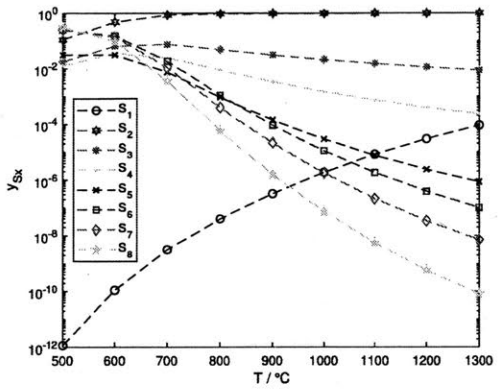

Figure 7-4: Equilibrium composition of sulfur gas as a function of temperature.

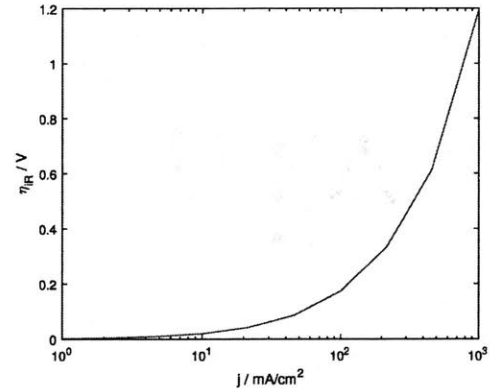

Figure 7-5: Ohmic overpotential for sulfur evolution

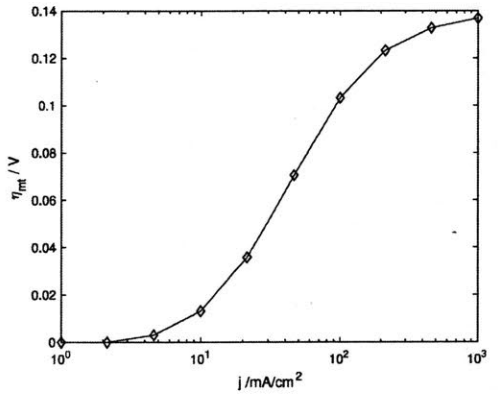

Figure 7-6: Mass transfer overpotential for sulfur evolution

substantially large ohmic overpotential. The resistance of the electrical leads is also included in this measurement. The ohmic overpotential does not grow superlinearly

with current density unlike the OER and CER cases.

The mass transfer overpotential was found to grow slowly at low current densities, increase in value rapidly at current densities near 50mA/cm^2, before ultimately slowing down at current densities near 1000mA/cm^2. Given that the concentration of S^{2-} is estimated to be ~30M, the entire anodic mass transfer overpotential for SER is expected to be due to supersaturation of S_2 near the electrode surface. Eq 7.2 provides a quantitative connection between the observed mass transfer overpotential, η_{mt} and the supersaturation of dissolved sulfur, $\frac{a_{S_2}^{surf}}{a_{S_2}^{bulk}}$:

$$\eta_{mt} = \frac{RT}{4F} \ln\left(\frac{a_{S_2}^{surf}}{a_{S_2}^{bulk}}\right) \tag{7.2}$$

Figure 7-7 suggests a limiting value of supersaturation of 75 is being approached. At

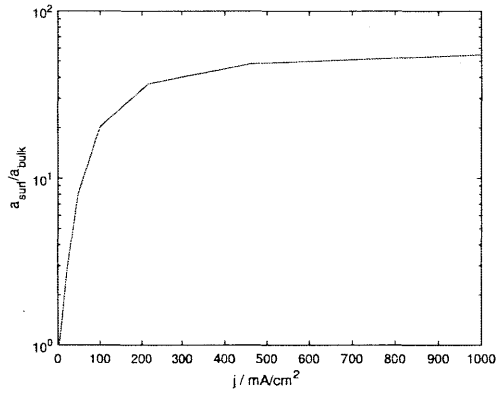

Figure 7-7: Supersaturation of S_2 observed in molten sulfide melt

the time of this study, the saturation concentration of S_2 is unknown in the electrolyte under study. Assuming convective mass transport from the electrode surface (j = $n_eF*n" = n_eFh_mC_{bulk}(\frac{C_s}{C_b}-1)$) still allows calculation of the quantity, $n_eFh_mC_b$, which can be thought of as the limiting current density for S_2 *reduction*. Figure 7-8 shows the variation of this "limiting" current density due to natural convection with the actual current density. The "limiting" current density grows with the applied current density because convection is increasing with actual current density. The sudden increase at ~200mA/cm^2 likely corresponds to the onset of significant bubbling at the electrode

surface which enhances convection. Assuming typical values of h_m (10^{-5}-10^{-4}m/s) suggests that the saturation concentration of S_2 in this electrolyte melt is 1-10mM. This range is about one order of magnitude larger than what is seen for O_2 in alkaline solutions and Cl_2 in molten halides. Given that physical gas solubility in molten salts is attributed to "holes" in the liquid [13], it would be expected that the smaller S_2 molecule would have a higher solubility than Cl_2 (molecular bond length of 189pm vs 199pm).

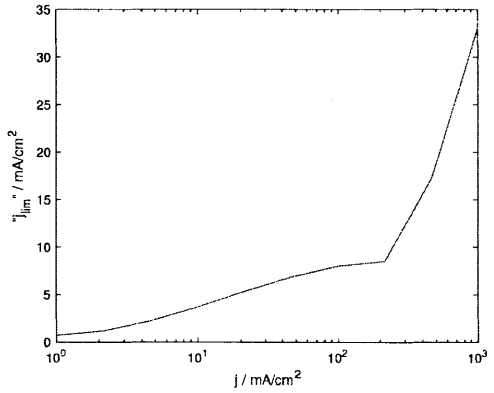

Figure 7-8: Variation of the "limiting" current density as S_2 evolution current density increases.

7.4 Summary

Characterization of SER with a graphite rod working electrode in a molten sulfide electrolyte of composition $(BaS)_{54}$-$(La_2S_3)_{36}$-$(Cu_2S)_{10}$ at 1300°C was carried out using the CI, and GEIS techniques. Key findings were:

- galvanostatic EIS showed negligible charge transfer resistance to the anodic reaction.
- the mass transfer overpotential initially increased quickly with current density before the rate of increase slowed as the current density approached 1000mA/cm^2.
- the supersaturation of S_2 in the vertical cylindrical electrode geometry appears to approach a limiting value of 75.

- solubility of S_2 in the electrolyte system is on the order of 1mM.

The overpotential behavior as a function of current density for SER was observed to have a similar magnitude but different shape compared to that in OER and CER. The next chapter will be devoted to comparing these systems and discussing the implications regarding hydrodynamic and thermodynamic properties of the molten sulfide system under study.

References

[1] C. Stinn, K. Nose, T. Okabe, and A. Allanore, "Experimentally Determined Phase Diagram for the Barium Sulfide-Copper(I) Sulfide System Above 873 K (600C)," *Metallurgical and Materials Transactions B*, vol. 48, no. 6, pp. 2922–2929, 2017.

[2] T. Lv, D. Chen, and M. Huang, "Quasiparticle band structures of BaO and BaS," *Journal of Applied Physics*, vol. 100, no. 8, pp. 0861031–0861033, 2006.

[3] P. E. Nikolaev and I. G. Vasileva, "Vapor pressure determination for solid and liquid La2S3 using boiling points," *Inorganic Materials*, vol. 44, no. 12, pp. 1367–1371, 2008.

[4] C. M. Forster and W. B. White, "Optical absorption edge in rare earth sesquisulfides," *Materials Research Bulletin*, vol. 41, pp. 448–454, 2005.

[5] K. Wakamura and I. Tsubota, "Small band gap and high ionic conduction in Cu S," *Solid State Ionics*, vol. 130, pp. 305–312, 2000.

[6] S. Sokhanvaran, S.-K. Lee, G. Lambotte, and A. Allanore, "Electrochemistry of Molten Sulfides: Copper Extraction from BaS-Cu2S," *Journal of The Electrochemical Society*, vol. 163, no. 3, pp. D115–D120, 2016.

[7] S. K. Sahu, B. Chmielowiec, and A. Allanore, "Electrolytic Extraction of Copper , Molybdenum and Rhenium from Molten Sulfide Electrolyte," *Electrochimica Acta*, no. 243, pp. 382–389, 2017.

[8] R. Kresse, U. Baudis, P. Jager, H. H. Riechers, H. Wagner, J. Winkler, and H. U. Wolf, "Barium and Barium Compounds," 2012.

[9] J.-C. G. Bunzli, "Lanthanides," 2013.

[10] A. Allanore, "Electrochemical engineering of anodic oxygen evolution in molten oxides," *Electrochimica Acta*, vol. 110, pp. 587–592, 2013.

[11] A. Allanore, "Features and challenges of molten oxide electrolytes for metal extraction," *Journal of the Electrochemical Society*, vol. 162, no. 1, pp. E13–E22, 2015.

[12] A. H. Caldwell, E. Lai, A. J. Gmitter, and A. Allanore, "Influence of mass transfer and electrolyte composition on anodic oxygen evolution in molten oxides," *Electrochimica Acta*, vol. 219, pp. 178–186, 2016.

[13] J. Lorimer, H. Clever, and C. Young, *Solubility Data Series: Gases in Molten Salts*, vol. 45. 1991.

Chapter 8

Discussion

Anodic gas evolution was studied in three very different environments: oxygen evolution at a Ni working electrode in 0.36M and 3.6M KOH aqueous solutions at room temperature, chlorine evolution at a glassy carbon working electrode in a LiCl-KCl-CsCl eutectic melt at 348°C, and sulfur evolution at a graphite working electrode in a Cu_2S-BaS-La_2S_3 melt at 1300°C. Care was taken to deconstruct the total measured overpotential into its ohmic, charge transfer, and mass transfer components, the last of which was of the greatest interest in understanding the chemistry of sulfur in a molten sulfide electrolyte by elucidating material properties of the sulfide melt which included the saturation concentration of dissolved sulfur gas, the limiting current density associated with the evolved gas, and the Schmidt number associated with dissolved sulfur.

8.1 Overpotentials present during OER, CER, and SER

While the mass transfer overpotential was the desired overpotential to study under conditions of fully developed fluid flow, the total overpotential (the sum of ohmic, charge transfer, and mass transfer overpotentials) was the measurable quantity during galvanostatic electrolysis. Table 8.1 below displays the different faradaic reactions

observed in the three systems studied, as well as the overpotentials measured in each case.

	OER	CER	SER
Rxn:	$4OH^- \rightarrow O_2 + 2H_2O + 4e^-$	$2Cl^- \rightarrow Cl_2 + 2e^-$	$2S^{2-} \rightarrow S_2 + 4e^-$
η_{iR}	iR_s	iR_s	iR_s
η_{ct}	$(R_{ct})^{-1} = \left(\frac{d(jA)}{d\eta_{ct}}\right)^*$	≈ 0	≈ 0
η_{mt}	$\frac{RT}{4F} \ln\left(\left(\frac{a^{surf}_{O_2}}{a^{bulk}_{O_2}}\right)\left(\frac{a^{surf}_{OH^-}}{a^{bulk}_{OH^-}}\right)^{-4}\right)$	$\frac{RT}{2F} \ln\left(\frac{a^{surf}_{Cl_2}}{a^{bulk}_{Cl_2}}\right)$	$\frac{RT}{4F} \ln\left(\frac{a^{surf}_{S_2}}{a^{bulk}_{S_2}}\right)$

Table 8.1: Overpotentials manifested during electrochemical oxygen, chlorine, and sulfur evolution.*the expression for jA is given in Eq 3.6

8.1.1 Ohmic overpotential

Ohmic overpotential in these three systems was shown to dominate at high current densities as reflected in Figures 5-4, 6-5, and 7-5. Bubble evolution showed a clear trend to increase the effective solution resistance as the nucleation rate (current density) increased. Visual confirmation that bubbles were indeed covering the electrode surfaces suggests that the local current density near the bubble layer increased. Average bubble sizes were found to increase in the order: $d_{O_2} < d_{Cl_2} < d_{S_2}$, with some Cl_2 and S_2 bubbles observed to be ~1mm in diameter. The surface tension of $KOH_{(aq)}$ under these conditions is 72.7mN/m (0.36M KOH) and 83.0mN/m (3.6M KOH). Though not measured for the eutectic chloride mixture that was studied, the surface tensions of LiCl, KCl, and CsCl are higher, ranging from 89mN/m-138mN/m at their respective melting points.[1]. This suggests similar values of surface tension for sulfur gas in the BaS-La_2S_3-Cu_2S electrolyte under study. Measurements of the contact angle of the electrolyte on graphite indeed showed significant non-wetting behavior of the electrolyte (see Appendix B).

8.1.2 Charge transfer overpotential

While not explicitly measured during the CER study, the charge transfer resistance for chlorine evolution has been reported to be negligibly small in simple molten alkali

chloride melts.[2, 3] Provided this assumption holds true, then the corresponding charge transfer overpotential is also negligibly small. The charge transfer resistance in the case of SER was measured via GEIS, and observed to be negligibly small as shown in Figure 7-3. Thus for all current densities studied for SER, there was no observable charge transfer overpotential. Unsurprisingly, low temperature OER experienced significant charge transfer overpotential as shown in Figure 5-5. While temperature effects can certainly explain the low rate of reaction, it is not uncommon to see charge transfer overpotential for oxygen evolution in molten systems.[4, 5] The lack of charge transfer overpotential during CER and SER suggests that the structure of the chloride and sulfide melts facilitates oxidation of the anions to their corresponding gases. Studies have shown that the electroactive species in simple alkali chloride melts is monatomic chloride, Cl^-. A similar lack of charge transfer overpotential in SER suggests that the electroactive species is free sulfide, S^{2-} rather than a polyatomic sulfide species.

8.1.3 Mass transfer overpotential

The mass transfer overpotential, as seen in Figures 5-6, 6-6, and 7-6 was found to be of similar magnitude for all three cases of gas evolution, though in the case of OER, was appreciably larger. This observation can be partially explained by the dilute nature of the reactant, OH^-, whose concentration was only 0.36M and 3.6M in this study. For comparison, the concentrations of reactant anions (Cl^- and S^{2-}) in the molten salt and molten sulfide cases were ~30M. Additionally, bubbles were found to vacate the electrode surface very rapidly such that immediately after the current was interrupted, the surface was almost free of bubbles.

CER exhibited a mass transfer overpotential dependence that grew linearly with the logarithm of the applied current density. Additionally, bubbles were found to stick to the electrode surface for a much longer time than in the aqueous case.

SER exhibited the lowest mass transfer potential. Unlike the other two systems, the rate of increase in the mass transfer overpotential with current density appear to slow as the current density approached $1000 mA/cm^2$.

Assuming that the mass transfer overpotential is dominated by the surface accumulation of gas (except in the case of aqueous OER, where mass transfer of the OH^- species was accounted for) it is possible to describe the degree of supersaturation of each gas as a function of current density. This is shown in Figure 8-1. Sulfur

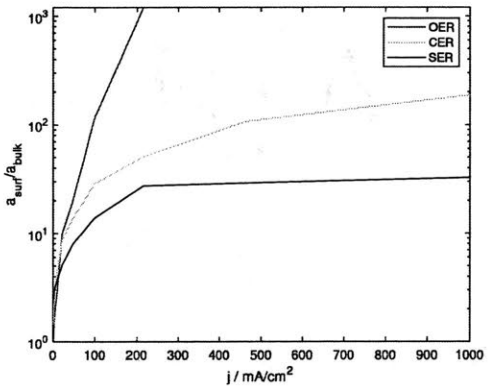

Figure 8-1: Supersaturation of all gases versus current density

is found to have the lowest degree of supersaturation. The elevated temperature of operation perhaps facilitates evaporation into the gaseous phase. The lower degree of supersaturation agrees with the previous finding that out of the three gases studied, the evolving sulfur bubbles were the largest in size. Considering the equilibrium of a species at the interface between the gaseous phase and the dissolved phase indicates that bubbles with lower radii of curvature correspond to lower degrees of supersaturation in the dissolved phase.

8.1.4 Properties of sulfur in the Cu_2S-BaS-La_2S_3 electrolyte system

The mass transport behavior of anodic sulfur evolution was found to effect a mass transfer overpotential of similar magnitude to that observed during OER in KOH_{aq} and CER in eutectic LiCl-KCl-CsCl. To a first approximation, this suggests that the physical properties governing fluid flow are rather similar. Considerations from the chemical engineering literature indicate that natural convective fluid flow is governed by two dimensionless parameters, namely the Grashof number, Gr (ratio of buoyancy

forces to viscous forces), and the Schmidt number, Sc (ratio of momentum diffusivity to chemical species diffusivity). Numerical simulations in Figure 8-2 show that at a fixed current density (or mass flux), the surface concentration of the evolved gas will decrease as the Sc number also decreases (as species diffusivity increases relative to momentum diffusivity). Sc numbers typical of aqueous systems are close to 1000 and in the molten salt studied, ~650. The Sc number for pure Cu_2S is roughly 200 at 1300°C. Given the lower observed supersaturation in SER vs OER and CER, it appears that the Sc number remains relatively unchanged around 200-300 upon mixing Cu_2S in the supporting electrolyte.

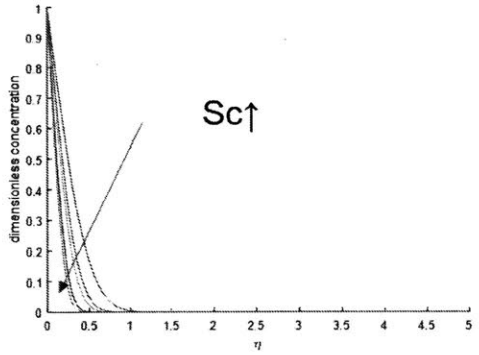

Figure 8-2: Non-dimensionalized concentration vs dimensionless distance from the electrode surface

The "limiting" current density for the reduction of S_2 is shown in Figure 7-8. This is straightforwardly calculated by dividing the applied current density by the observed supersaturation at each current density. It was found that this limiting density grew with current density, a result expected from natural convection driven flow where the rate of convection increases with current density due to an ever increasing density gradient near the electrode surface as well as the onset of bubble nucleation.

If one assumes a similar growth behavior of the convective mass transfer coefficient with respect to current density as observed during CER (Figure 6-8, then from the limiting current density for SER, one can approximate the saturation concentration of S_2 as this value remains fixed independent of the current density. The resulting saturation value is ~3mM in the studied electrolyte.

8.2 Perspectives and future work

This work demonstrated the materials-blind applicability of electrochemistry to characterize vastly different systems in terms of both chemistry and temperature. In the process of understanding the underlying chemistry and hydrodynamics involved during SER, certain electrochemical engineering considerations were obtained that can assess the potential utility of molten sulfide electrolytes for industrial production of metal from sulfide-based ores and guide future design of MSE cells. These considerations are listed below:

- Graphite serves as an inert anode capable of sustaining sulfur gas evolution at high current densities ($>1 A/cm^2$).

- Mass transfer overpotential at the anode during SER is comparable to that of CER in molten chlorides and OER in aqueous KOH. Due to the higher temperature of operation, this implies a lower degree of supersaturation of dissolved sulfur gas than chlorine or oxygen.

- The saturation concentration of sulfur appears to be larger than typical gas-electrolyte systems. This suggests that the potential for back reaction with the cathode product is higher if the metal is also soluble in the molten sulfide electrolyte. Thus gas removal at the anode surface is of paramount importance. This highlights the need for proper cell design with vertical electrodes.

- Charge transfer kinetics at the temperature of operation for SER are negligibly small, thus the current density distribution will be dominated by the primary current distribution and potentially tertiary current distribution if gas removal is not optimized.

The author can envision many different paths down which to extend this work. A few are mentioned below.

8.2.1 Electrolyte composition

Extension of the electrochemical techniques and analysis to other compositions of molten sulfides would allow for better understanding of the role of the transition metal cations. *Physical* solubility of chlorine in molten salts and *physical* solubility of oxygen in molten oxides span many orders of magnitudes.[6, 7] It would be interesting to see if sulfur behaves similarly in molten sulfides where *chemical* solubility could be important, such as in systems with mixed valency metal ions. One would expect the supersaturation to decrease in such systems as homogeneous chemical reaction would reduce the surface concentration of dissolved sulfur.

8.2.2 Cell geometry

The measurements of mass transfer overpotentials in this study were measured with relatively ideal geometries where mass transfer at the counter electrode (cathode) would not influence the mass transfer observed at the anode. It would be interesting to observe the affect of anode-cathode distance on the overpotential behavior. The amount of back reaction between sulfur and the metallic product would greatly be influenced by the prevailing flow conditions - a critical element to designing an optimal electrochemical cell.

8.2.3 Reference electrode

While graphite and tungsten maintained stable quasi-reference potentials on the time scale of the measurements made, there remains a strong desire to establish a true reference electrode, especially in sulfide melts that contain mixed valency metal ions.

8.2.4 Anode

Graphite was determined to function as an inert anode in the molten sulfide electrolyte systems studied. Having an inert anode greatly facilitates electrochemical reactor design as maintaining a constant anode-cathode-distance is much easier than with a

consumable anode. However, the wettability of the electrolytes studied on graphite was rather poor- contact angle measurements performed in the floating zone furnace revealed three phase contact angles of >105°. This finding helps explain the frequent observation that large sulfur gas bubbles were trapped on the anode surface during electrolysis. Finding a metal/metal composite inert anode with better wettability is expected to improve the efficiency of sulfur gas removal.

8.3 Selectivity

Electrochemistry provides a powerful tool to discriminate against unwanted side reactions. One of the merits of utilizing a molten sulfide supporting electrolyte instead of a halide based salt to electrowin a sulfide based ore is favorable selectivity - there is no competition between sulfide and halide oxidation in the molten sulfide. Interestingly, common anion impurities in sulfide based ores include arsenides, tellurides, and selenides. Thermodynamically, these species are less stable than sulfides and should be oxidized at less positive potentials than the sulfide ion. Thus careful control of the current density at the anode should allow for selective oxidation and impurity removal. This concept was proven at the cathode where selective reduction of cation impurities was demonstrated by Sahu and the author.[8] ReS_2 and MoS_2 were added in addition to Cu_2S to the supporting electrolyte. At the lowest current densities, only metallic Re was found at the cathode. At intermediate current densities, Re+Mo was found at the cathode. At larger current densities, all three metals were found deposited at the cathode. This finding confirmed the Ellingham diagram predictions for the decomposition potentials of the three transition metal sulfides involved. A similar study involving anion impurity removal at the anode should be pursued.

8.3.1 Summary

Electrochemical impedance techniques allows for the isolation of three main sources of overpotential (ohmic, charge transfer, and mass transfer) during electrolytic gas evolution in aqueous KOH, molten chloride, and molten sulfide electrolyte solutions.

By comparing the magnitude and current density dependence of the mass transfer overpotential in all three cases, insights into the previously unknown chemical and hydrodynamic properties of sulfur in a molten sulfide electrolyte were obtained, most notably, the saturation concentration of S_2 in the studied molten sulfide electrolyte, the Schmidt number, as well as the "limiting" current density in an idealized geometry. These finding are integral to our growing understanding of the fundamental electrochemistry at play during molten sulfide electrolysis.

References

[1] A. H. Ayyad, "On the surface tension of molten salts and its temperature dependence," *Physics and Chemistry of Liquids*, vol. 55, no. 1, pp. 120–130, 2017.

[2] A. E. Din, "Molten salt electrolysis - I. Chlorine over-potential on carbon in LiCl-KCl eutectic," *Electrochimica Acta*, vol. 4, no. August 1960, pp. 242–250, 1961.

[3] I. G. Murgulescu, S. Sternberg, L. Medintev, and C. Mustetea, "Overvoltage and depolarization in molten AgCl, AgBr and AgI," *Electrochimica Acta*, vol. 8, no. 1-2, pp. 65–75, 1963.

[4] H. Flood and T. Forland, "Some Investigations on the Oxygen-Overpotential in Molten Salts," *Discussions of the Faraday Society*, vol. 1, pp. 302–307, 1947.

[5] G. J. Janz, F. Colom, and F. Saegusa, "Oxygen Overpotential in Molten Carbonates," *Journal of The Electrochemical Society*, vol. 107, no. 7, pp. 581–586, 1960.

[6] J. Lorimer, H. Clever, and C. Young, *Solubility Data Series: Gases in Molten Salts*, vol. 45. 1991.

[7] R. H. Doremus, "Diffusion in glasses and melts," *Journal of Non-Crystalline Solids*, vol. 25, no. 1-3, pp. 261–292, 1977.

[8] S. K. Sahu, B. Chmielowiec, and A. Allanore, "Electrolytic Extraction of Copper , Molybdenum and Rhenium from Molten Sulfide Electrolyte," *Electrochimica Acta*, no. 243, pp. 382–389, 2017.

Appendix A

AC Voltammetry Study

Without visual access to the anode surface during SER, it is quite desired to have supplementary means of detecting electrolytic gas evolution to confirm that the Faradaic reaction under study is indeed gas evolution. Large electrode double layer capacitances and inductive electrical leads are quite common in high temperature electrochemical experiments. These non-Faradaic phenomena can complicate the analysis of DC electrochemical techniques like cyclic voltammetry. Large Amplitude Fourier Transform Alternating Current Voltammetry (LA-FT-ACV) provides a method to isolate the Faradaic response at an electrode surface by catering to the non-linear dependence of the Faradaic current on potential perturbation. The interested reader should consult the literature [1–6] to fully understand the theoretical development of the technique which is outside the scope of this work. While first developed in low temperature aqueous systems, the technique has been extended to concentrated, high temperature molten electrolytes, including chlorine evolution in a molten chloride melt and oxygen evolution in molten oxide melts.[7] LA-FT-ACV was employed in addition to the CI and GEIS techniques in this study to characterize SER at both the scale of the CI and GEIS measurements, as well as in a floating zone furnace which gave visual access to the electrodes and electrolyte during the experiment.

A.1 Materials and equipment

The electrolyte and electrodes and furnace were the same as those used in Section 7.2. An additional set of experiments were also performed inside of a floating zone furnace (Crystal Systems Corp, TX-12000-I-MIT-VPO-PC). At this smaller scale, only 100mg of electrolyte were used. The electrolyte sample was a a 100mg solid piece broken off the premelted rod of electrolyte. A schematic of the floating zone furnace and picture of the sample are presented in Figure A-1. LA-FT-ACV measurements were made with a potentiostat (Gamry, Reference 3000) coupled with an ultra-low distortion arbitrary waveform generator (Stanford Research Systems, DS360) and high sampling rate data acquisition (DAQ) module (Data Translation, DT9837B). A schematic of the electrical setup is shown in Figure A-2. Coaxial cables connected the output of the waveform generator to the external excitation input of the potentiostat. The analog output signals of the working electrode potential and the current were connected via coaxial cables to the DAQ and recorded using the proprietary software, QuickDaq.

A.2 Electrochemical methods

The operating parameters tested during LA-FT-ACV measurements are presented below in Table A.1. These same parameters were used both during the large scale experiment and small scale in the floating zone furnace.

f	3.98, 39.8, 398Hz
ΔE	120mV
ν	3mV/s

Table A.1: ACV parameters utilized during the study of SER at a graphite working electrode

A.2.1 Results and discussion

Identical measurements were made in both the large scale (46g) and small scale (100mg) systems (the parameters listed in Table A.1). The 2nd and 3rd harmonic

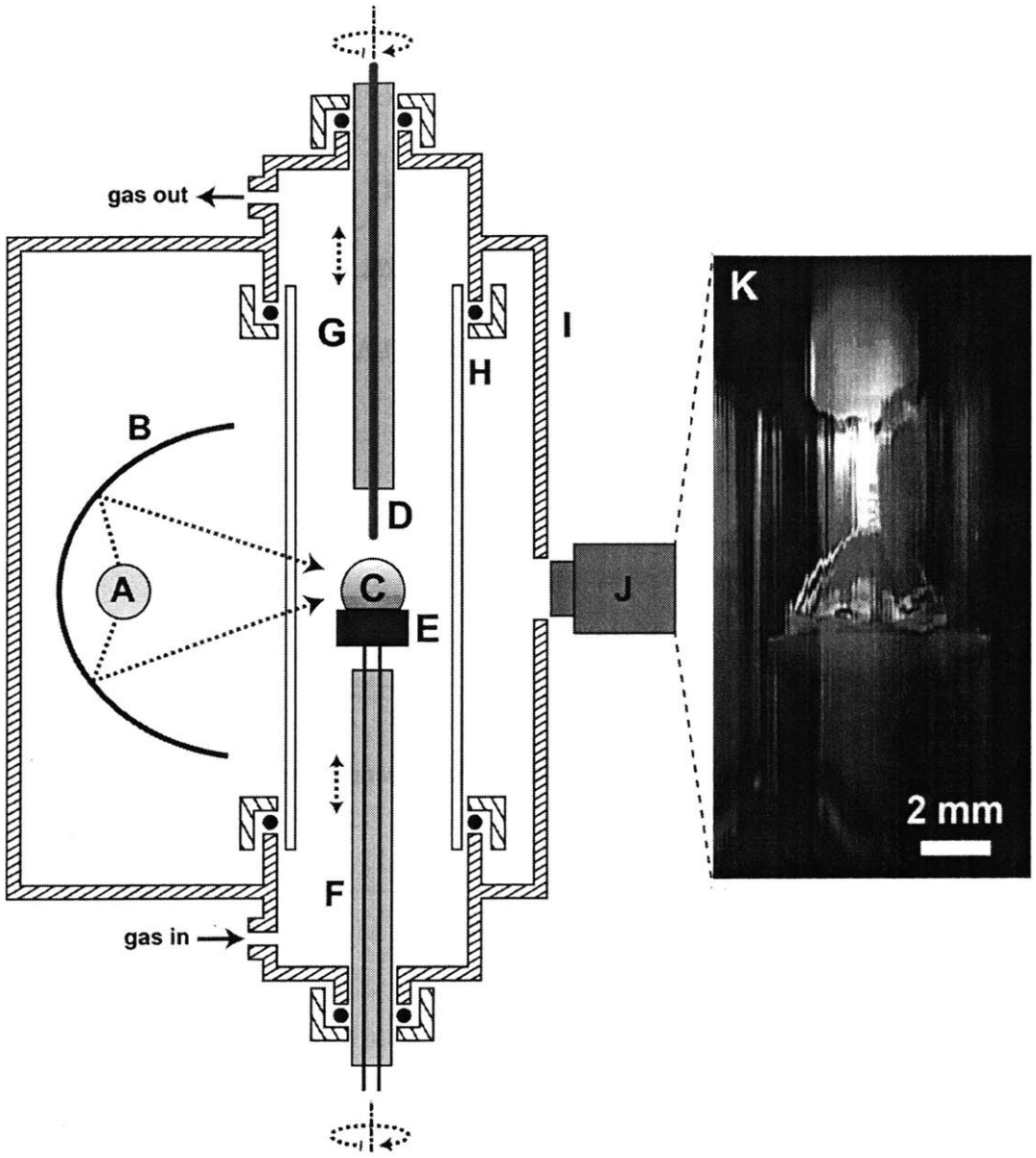

Figure A-1: Left) Schematic of floating zone furnace. (A) Xe lamp and (B) ellipsoidal mirror (one of four shown), (C) molten droplet (0.1mL volume, typically) in the hot zone, (D) solid metallic rod acting as cathode, (E) anode + electrolyte support, (F) electrode leads and lower shaft, (G) electrode lead and upper shaft, (H) quartz tube, (I) furnace shell, (J) camera. Right) Sample droplet of molten sulfide electrolyte sitting upon graphite working electrode.

current responses for the large scale and small scale systems are shown below in Figure A-3 and Figure A-4, respectively.

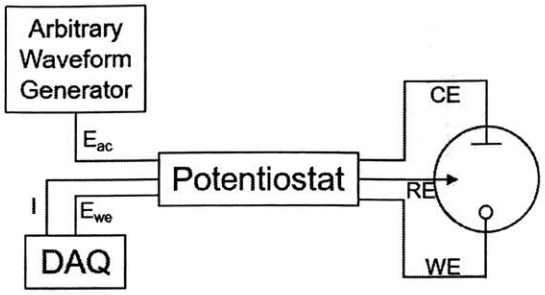

Figure A-2: Electronic configuration for performing LA-FT-ACV measurement.

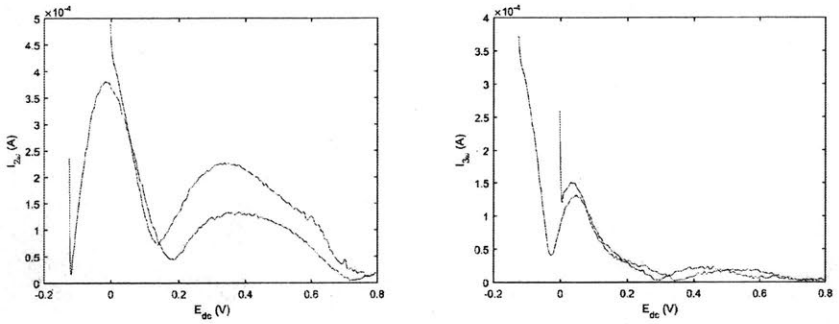

Figure A-3: 2nd (left) and 3rd (right) harmonic current responses during SER in large scale molten sulfide electrolyte

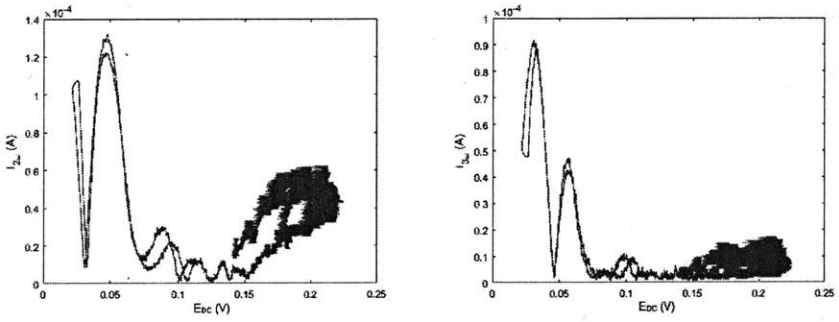

Figure A-4: 2nd (left) and 3rd (right) harmonic current responses during SER in small scale molten sulfide electrolyte

There is marked similarity between the two cases. The well defined peaks are indicative of a fast redox reaction. The wider peaks in the large scale measurement is likely due to uncompensated resistance affecting the reported DC potential. In order to see harmonic responses to the AC perturbation, a sufficiently high excitation frequency was required. There was no signal above the noise when excitation frequencies

of 3.98Hz and 39.8Hz were used - only 398Hz produced a non-linear response during SER. The matching behavior evidences the ACV technique's ability to span different length scales and geometries.

Nakanishi [7] observed similar harmonic current responses while utilizing LA-FT-ACV to study CER in eutectic NaCl-KCl and OER in molten Al_2O_3 and molten mixtures of La_2O_3-Y_2O_3. The matching behavior gives strong evidence that the molten sulfide electrolyte indeed enables the oxidation of sulfide anions to $S_{2(g)}$.

References

[1] D. E. Smith, "AC polarography and related techniques," in *Electroanalytical Chemistry: A Series of Advances (I)* (A. J. Bard, ed.), ch. 1, pp. 1–155, New York: Marcel Dekker, Inc., 1966.

[2] A. Bond, R. O'Halloran, I. Ruzic, and D. Smith, "Fundamental and Second Harmonic Alternating Current Cyclic Voltammetric Theory and Experimental Results for Simple Electrode Reactions Involving Solution-Soluble Redox Couples," *Analytical Chemistry*, vol. 48, no. 6, pp. 872–883, 1976.

[3] S. O. Engblom, J. C. Myland, and K. B. Oldham, "Must AC Voltammetry Employ Small Signals?," *Journal of Electroanalytical Chemistry*, vol. 480, no. 1-2, pp. 120–132, 2000.

[4] D. J. Gavaghan and A. M. Bond, "A complete numerical simulation of the techniques of alternating current linear sweep and cyclic voltammetry: analysis of a reversible process by conventional and fast Fourier transform methods," *Journal of Electroanalytical Chemistry*, vol. 480, no. 1-2, pp. 133–149, 2000.

[5] A. Bond, N. Duffy, S. Guo, J. Zhang, and D. Elton, "Changing the Look of Voltammetry," *Analytical Chemistry*, vol. 77, pp. 186A–195A, 2005.

[6] A. M. Bond, D. Elton, S. X. Guo, G. F. Kennedy, E. Mashkina, A. N. Simonov, and J. Zhang, "An integrated instrumental and theoretical approach to quantita-

tive electrode kinetic studies based on large amplitude Fourier transformed a.c. voltammetry: A mini review," *Electrochemistry Communications*, vol. 57, pp. 78–83, 2015.

[7] B. R. Nakanishi and A. Allanore, "Electrochemical study of a pendant molten alumina droplet and its application for thermodynamic property measurements of Al-Ir," *Journal of The Electrochemical Society*, vol. 164, no. 13, pp. E460–E471, 2017.

Appendix B

Selected properties of the studied electrolyte systems

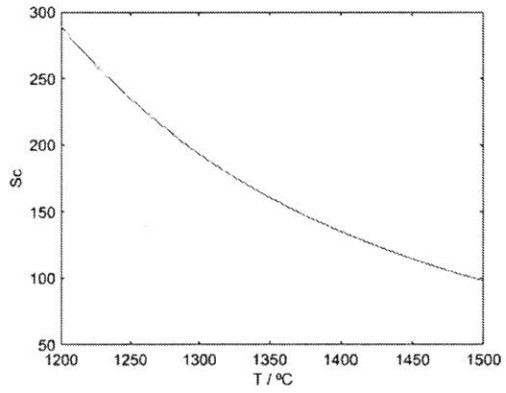

Figure B-1: Pure Cu_2S Sc number vs temperature

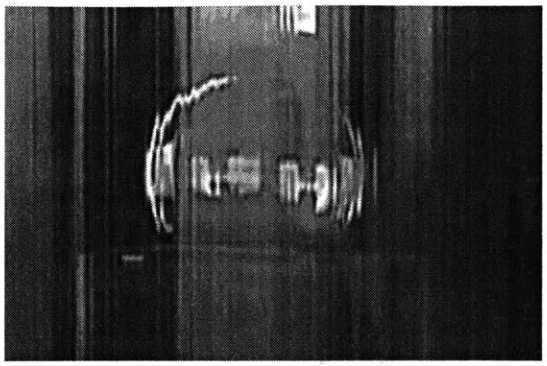

Figure B-2: Contact angle measurement of BaS-La_2S_3 electrolyte on graphite as measured by floating zone furnace. The three-phase contact angle was measured to be 104°+/-2°, indicating poor wetting of graphite

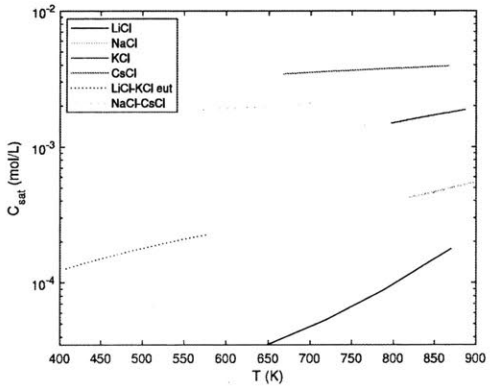

Figure B-3: Saturation concentration of Cl_2 in select alkali chlorides

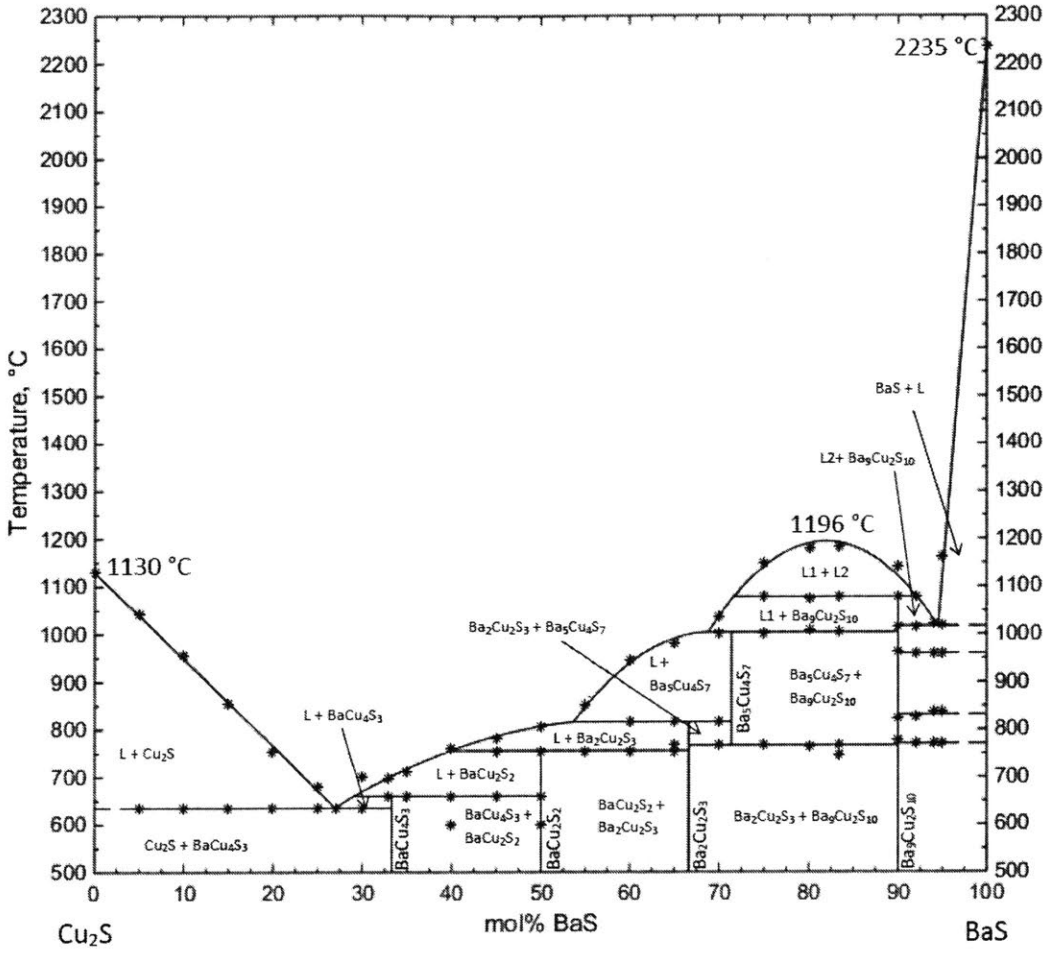

Figure B-4: BaS-Cu_2S Phase Diagram

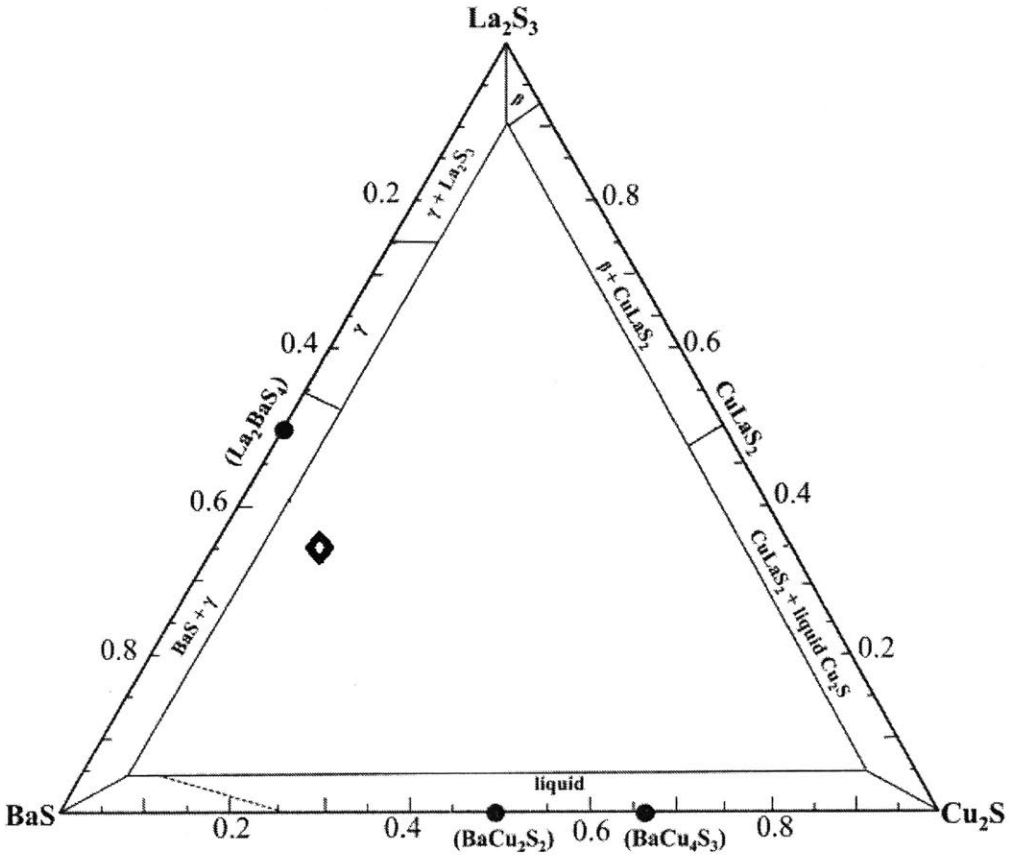

Figure B-5: BaS-La_2S3-Cu_2S Phase Diagram - diamond indicates electrolyte composition under study